Redox control on chromium isotope behaviour in silicate melts in contact with magnesiochromite

P. Bonnand, Emilie Bruand, A.K. K Matzen, M. Jerram, Federica Schiavi,
B.J. J Wood, M. Boyet, A.N. N Halliday

Redox control on chromium isotope behaviour in silicate melts in contact with magnesiochromite

P. Bonnand[1,2*], E. Bruand[1,2], A.K. Matzen[2], M. Jerram[2,3], F. Schiavi[1], B.J. Wood[2], M. Boyet[1] and A.N. Halliday[2,3]

[1]Université Clermont Auvergne, CNRS, IRD, OPGC, Laboratoire Magmas et Volcans, F-63000 Clermont-Ferrand, France.

[2]Department of Earth Sciences, University of Oxford, South Parks Road, Oxford, OX1 3AN, United Kingdom.

[3]The Earth Institute, Columbia University, 2910 Broadway, New York, NY 10025 USA.

*Corresponding author

Present address, Université Clermont Auvergne, CNRS, IRD, OPGC, Laboratoire Magmas et Volcans, F-63000 Clermont-Ferrand, France.

Email address: pierre.bonnand@uca.fr

Tel. No: +33 (0)473346783

27   Abstract:

28

29   Transition metal isotopes are particularly useful for understanding the conditions under which

30   magmatic processes occur. Moreover, those with more than one oxidation state (e.g. Cr^{2+},

31   Cr^{3+} and Cr^{6+}) may also provide powerful constraints on the evolution of the redox state of the

32   mantle over time. By investigating the Cr isotopic compositions in both magnesiochromite

33   and silicate melts during experiments performed at 1300 °C and under controlled redox

34   conditions ($-12 < \log f O_2 < -4$), this study presents the first experimental petro-isotopic

35   investigation of Cr isotope fractionation and reveals clear systematics between Cr

36   concentration, isotopic compositions and $f O_2$. Two series of experiments were performed to

37   study (a) the dissolution of a natural magnesiochromite into Cr-free silicate melts (series A)

38   and (ii) the crystallisation of magnesiochromite from Cr-doped silicate melts (series B). In

39   agreement with previous studies, the Cr solubility in the silicate melts at equilibrium with

40   magnesiochromite is strongly controlled by oxygen fugacity. Melts produced at low $f O_2$ are

41   enriched in Cr compared to more oxidised melts. In series A experiments, the Cr isotopic

42   composition of silicate melts are lighter than the initial chromite starting material. The

43   experiments, performed at $-12 < \log f O_2 < -6$, reveal that Cr isotopic compositions of the

44   silicate melts are correlated with $f O_2$. This demonstrates that, as for the Cr solubility, Cr

45   isotopes are sensitive to $f O_2$ and could be used to track changes in redox conditions in high-

46   temperature processes. Furthermore, the Cr isotopic compositions of silicate melts that are

47   reacted under more oxidising conditions ($\log f O_2 > -6$) are much lighter than those of melts

48   equilibrated with magnesiochromite at lower oxygen fugacity. The observed variations can be

49   explained by changes in bonding environment for Cr under oxidised conditions in the silicate

50   melts and/or in the magnesiochromite grains. Similarly, the second set of experiments

51   designed to study fractional crystallisation (series B) suggest that Cr isotope fractionation is

52   larger under oxidising conditions.

53

54

55

56

57   Keywords: Cr isotopes, Redox conditions, Magnesiochromite, partial melting, fractional
58   crystallisation

59 1. Introduction

60

61   Transition metals are useful for understanding the conditions of differentiation processes

62 such as core formation (e.g. Bourdon et al. 2018). Elements with more than one oxidation

63 state can also provide powerful constraints on the evolution of the redox conditions in the

64 mantle through time (e.g. Williams et al. 2004). The ability to determine isotopic

65 fractionations associated with such differentiation processes has provided new tools whereby

66 early Earth conditions can be explored. Chromium (Cr) is of particular interest because it can

67 be present in two main oxidation states in silicate melts (Cr^{2+} and Cr^{3+}), although during

68 quenching Cr^{2+} is oxidised by Fe^{3+} and only Cr^{3+} has been measured in room-temperature

69 silicate glasses (Berry and O'Neill 2004). Chromium isotopic compositions have been

70 measured in a number of terrestrial and extra-terrestrial samples (e.g. Schoenberg et al. 2008,

71 Moynier et al. 2011, Farkas et al. 2013, Wang et al. 2016, Bonnand et al. 2016a, Bonnand et

72 al. 2016b, Schoenberg et al. 2016, Xia et al. 2017, Bonnand and Halliday 2018, Shen et al.

73 2018, Shen et al. 2020, Bonnand et al. 2020). However, very little experimental work has

74 been done to independently verify the isotopic effects found in nature. The aim of this study is

75 to investigate the impact of oxygen fugacity on the behaviour of Cr and its isotopic

76 compositions during partial melting and fractional crystallisation in a basaltic system. To this

77 end, the Cr isotopic compositions of silicate melts and chromite have been measured in the

78 run products of 1-atm experiments performed under controlled oxygen fugacity.

79 2. Background

80   2.1. Chromium in the mantle and in silicate melts

81   The Cr concentrations in terrestrial basalts are highly variable and can be up to 2000 µg

82 g^{-1} (e.g. Maclennan et al. 2003). The Cr concentration in mantle peridotites is also variable

83 ranging from 1000 µg g^{-1} to about ~4000 µg g^{-1} (e.g. Bodinier and Godard 2013 and

84 references therein). In basaltic and peridotitic systems, Cr-bearing minerals are spinel, garnet,

85 orthopyroxene and clinopyroxene. During partial melting, Cr is a compatible element

86 meaning that Cr concentrations in the melt are lower than that of the solid residue. The

87 solubility of Cr in the silicate melt is mainly controlled by the partition coefficient between

88 spinel and/or garnet and the silicate melts. The crystal-melt partition coefficient ($D_{crystal-melt}$) of

89 Cr into spinel (~ 170, Liu and O'Neill 1994) is higher than that of garnet (~ 5.5, McKenzie

90 and O'Nions 1995) and this suggest that melts produced at higher pressure should be enriched

91 in Cr compared to silicate melts produced at low pressure (e.g. Bonnand et al. 2020). During

92   fractional crystallisation in basaltic systems, Cr is mainly hosted in spinel and clinopyroxene

93   depending on the chemical composition of the silicate melt and the temperature of

94   crystallisation.

95   The presence of Cr^{2+} in silicate melts has been demonstrated by in-situ XANES

96   measurements, performed by Berry et al. (2006). They also show that the ratio Cr^{2+}/Cr_{TOT}

97   varies with oxygen fugacity and the chemical composition of the silicate melts. The solubility

98   of chromium in silicate melts is dependent on temperature, oxygen fugacity and the chemical

99   composition of the silicate melt (Roeder and Reynolds 1991, Hanson and Jones 1998, Huang

100   et al, 2019). A number of experimental studies have demonstrated that Cr^{2+} is more soluble

101   than Cr^{3+} (e.g. Murck and Campbell 1986). The Cr solubility in silicate melts increases under

102   reduced conditions (from 0.072 Cr_2O_3 wt % at $\log fO_2 = - 5.1$ to 1.43 wt. % at $\log fO_2 = -12.78$,

103   Roeder and Reynolds 1991). This observation is consistent with high Cr concentration in the

104   lunar basalts, compared with their terrestrial counterparts. Chromium solubility also increases

105   with temperature (at $\log fO_2 = -8$, from 0.085 wt % at 1200 ˚C to 0.162 wt. % at 1300 ˚C,

106   Roeder and Reynolds 1991, Hanson and Jones 1998). In silicate melts, Cr^{3+} is octahedrally

107   coordinated whereas Cr^{2+} is located in a distorted octahedral site (Keppler 1992).

2.2. Chromite

109   In ultramafic and mafic magmatic reservoirs, the main Cr-bearing phases are spinel and

110   pyroxene. There are two types of spinel minerals: 2-3 spinels such as $MgAl_2O_4$ and $MgFe_2^{3+}$

111   O_4 and 2-4 spinels such as Fe_2TiO_4 and the high pressure form of Mg_2SiO_4 (Biagioni and

112   Pasero 2014). Chromite is a 2-3 spinel-structured oxide, common in a variety of rocks such as

113   mantle xenoliths and basalts but also in metamorphic and sedimentary rocks (Dick and Bullen

114   1984). The 2-3 spinel structure $A^{2+}B^{3+}_2O_4$ is based on a nearly ideal cubic close-packed array

115   of oxygen atoms with tetrahedral and octahedral sites. The cations in the tetrahedral sites (A,

116   IV fold coordinated) are usually Mg^{2+}, Fe^{2+}, Zn^{2+}, Mn^{2+}. The cations in the octahedral sites

117   (B, VI fold coordinated) are Al^{3+}, Fe^{3+} and Cr^{3+}. The spinel structure can be modified to

118   accommodate the presence of high Fe^{3+} concentration (e.g. Lenaz and Lughi 2013). In this

119   case the Fe^{3+} can move to the A site and this structure is referred to as inverse spinel. It is

120   commonly assumed however, that magnesiochromite has a normal spinel structure. The

121   normal and inverse structures are two end-members which form a continuum and depending

122   on the chemical composition and the physical conditions, 3+ cations can migrate to the A site.

123   It is important to note, however, that the spinel structure is such that it can host a large

124   number of trace elements including transition metals and high-field-strength elements (HFSE)

(Nielsen et al. 1994). With such high partition coefficients, spinel plays an important role in the trace element budget in most natural igneous rocks, despite relatively low modal proportions. For example, spinel controls the behaviour of many transition metals during partial melting and fractional crystallisation (e.g. Li et al. 1995). Indeed, chromite is often associated with economically important platinum group element (PGE) deposits (Naldrett et al. 2009).

The variations in the chemical compositions of natural chromite has attracted a lot of attention and several parameters are commonly used to describe the observed compositions:

$$Cr\# = Cr^{3+} / (Cr^{3+} + Al^{3+})$$

$$Fe^{3+}\# = Fe^{3+} / (Cr^{3+} + Al^{3+} + Fe^{3+})$$

$$Mg\# = Mg^{2+} / (Mg^{2+} + Fe^{2+})$$

where Cr^{3+}, Al^{3+}, Fe^{3+}, Fe^{2+} and Mg^{2+} are atomic abundances calculated assuming 4 oxygen atoms in the spinel structure and that Cr is only present as Cr^{3+}. In natural spinel, there are large compositional variations between several endmembers and these variations have been linked to the chemical compositions of basalts and/or peridotite, crystallisation temperature, and pressure (e.g. Warren 2016). A number of previous studies have shown that partitioning of transition metals and/or HFSE between spinel/chromite and melts depends on temperature, pressure and the chemical composition of the crystal and melt (Nielsen et al. 1994, Horn et al. 1994, Nielsen and Beard 2000, Blundy and Wood, 2003, Righter et al. 2006, Davis et al. 2017). Redox state also plays a major role in controlling the chemical composition of natural chromite and many experimental studies have calibrated these variations (e.g. Wood et al. 1990, Frost and McCammon, 2008). Although chromite plays a major role in controlling the Cr behaviour in magmatic system, no experimental work has been conducted on the impact of chromite on the behaviour of Cr isotopes.

2.3. Chromium isotopes

The variations in Cr isotopes are reported using the notation:

$$\delta^{53}Cr = (\frac{^{53}Cr/^{52}Cr_{sample}}{^{53}Cr/^{52}Cr_{NIST\ SRM\ 979}} - 1) \times 1000$$

Most recent analyses on mantle xenoliths and mineral separates have shown that Cr isotopes are fractionated during partial melting (Xia et al. 2017, Farkas et al. 2013, Bai et al. 2019). The residues become heavier while partial melting proceeds and the melts are therefore

5

believed to be lighter than the residues (Xia et al. 2017, Shen et al. 2018). Furthermore, data

from mineral separates reveal that, at equilibrium, the Cr isotopic compositions become

heavier in the order olivine ≤ cpx = opx < spinel (Shen et al. 2018). It has also been

demonstrated that Cr isotopes are fractionated during magmatic differentiation on Earth and

on the Moon (Bonnand et al. 2020, Shen et al. in 2020, Bonnand et al. 2016b). Recently, it has

been proposed that the isotopic fractionation occurring during fractional crystallisation

depends on the the Cr^{3+}/Cr_{TOT} ratios in both the silicate melts and the crystallising phases

(Farkas et al. 2013, Schoenberg et al. 2016, Bonnand et al. 2020, Shen et al. 2020). The Cr

isotopic variations in HED (Howardite–Eucrite–Diogenite) have also been linked to magmatic

processes as well as Cr volatility during planetary accretion (Zhu et al. 2019). Comparing Cr

isotope signatures in samples from different planetary bodies is complicated further by the

fact that processes active during planet formation may have affected the isotopic compositions

of the major reservoirs. For example, the observed difference in Cr isotopes (δ^{53}Cr) between

the Moon and the Earth has been attributed to the volatility of Cr during the late stages of the

Moon forming Giant Impact (Sossi et al. 2018). In several studies, the variations observed in

Cr isotopes in silicate melts and mantle xenoliths have been linked to the isotopic composition

of chromite (Farkas et al. 2013, Xia et al. 2017, Shen et al. 2018, Bonnand et al. 2016,

Bonnand et al. 2020, Shen et al. 2020). Our ability to estimate the Cr isotopic composition of

silicate reservoirs is hampered by our limited understanding of the fractionation factors in

high-temperature processes.

3. Analytical methods
    3.1. Experiments

    The starting compositions used in this study are listed in Table 1. These compositions were

synthesised using reagent-grade oxide powders, which were mixed by grinding under ethanol

in an agate mortar and pestle.

    Two series of experiments were conducted during the course of this study. The first (series

A) was designed to study the dissolution of chromite into a Cr-free silicate melt. The second

(series B) was designed to study the fractional crystallisation of chromite out of the silicate

melts. The only chemical difference between the two silicate melts used in this study is the Cr

concentration (see Table 1). The bulk compositions of the melts were chosen such that they

were completely molten at 1300°C. To avoid Fe loss from the silicates, loops were pre-

saturated by performing multiple saturation experiments (e.g. Hanson and Jones, 1998). We

189 performed three saturation experiments (72 h per experiment) for each loop at the required

190 temperature and fO$_2$.

191   For each series A experiment, 100 mg of starting material A and 5 mg of natural chromite

192 grains (50-200 µm) were combined and pressed into a small pellet (~4 mm diameter). For

193 each series B experiment, 100 mg of starting material B was weighed and pressed into a small

194 pellet. Experimental conditions (e.g. oxygen fugacity, loop material) for each experiment are

195 given in Table 2. Using the series A experimental method, we performed a time series, using a

196 single Pt loop. The loop was used to perform 5 experiments (A3a, A3b, A3c, A3d and A3)

197 with run durations from 2 h to 168 h (Table 2). Between each run, the silicate material was

198 removed and the loop was cleaned in a cold bath of concentrated HF. In addition to the time

199 series, six experiments were performed using method A (A1 to A7), and three experiments

200 were performed using method B (B1 to B3). For each series, the experiment number is given

201 with increasing oxygen fugacity (i.e. A1 is the experiment performed under the more reducing

202 conditions for the series A experiments).

203   Experiments were performed at the Department of Earth Sciences of the University of

204 Oxford. A schematic is presented in Fig. 1. The experiments were performed by holding the

205 powdered starting material in the hot spots of a gas-mixing furnace (Fig. S1). During the

206 experiments, the temperature was controlled to within ± 5 °C of the desired temperature (1300

207 °C), and monitored by a thermocouple adjacent to the sample. Oxygen fugacity was

208 controlled using flowing CO and CO$_2$. Experiments were performed from two log units below

209 to six log units above the Iron-Wüstite (IW) buffer. An O$_2$ sensor, made of yttria-stabilized

210 zirconia, was used to monitor the oxygen fugacity during the duration of each experiment.

211 The measured fO$_2$ is thought to be accurate to within 0.1 (1 s.d.) log units. Depending on

212 oxygen fugacity, starting materials were suspended using Pt or Re-loops. The samples for

213 series A experiments were slowly placed into the furnace at 800°C, the temperature was then

214 increased to 1300°C where it was held for 168 h. The experimental procedure was similar for

215 the series B experiments except, in order to facilitate the crystallization of chromite,

216 temperature cycling was employed at the beginning of the experiment. After insertion into the

217 furnace the temperature was increased to 1550 °C, followed by cooling to 1300 °C at 5 °C h^{-1};

218 the temperature was increased again to 1450 °C followed by cooling to 1300 °C at 5°C h^{-1}

219 after which the temperature was kept constant (at 1300 °C) for 168 h. At the end of all

220 experiments, samples were quenched by dropping them into water.

221   Previous studies have reported Cr loss during experiments performed both at high and low

222 fO$_2$ (Hanson and Jones 1998). While Cr loss at low fO$_2$ is likely due to Cr entering the loop,

223 Cr volatility was observed in experiments performed in air ($\log f O_2 = -0.68$, Hanson and Jones
224 1998), an $f O_2$ that is higher than those used in this study ($\log f O_2$ range from -12 to -4). More
225 recently, Sossi et al. (2019) proposed that Cr is volatile at 1-atm under oxidizing conditions
226 ($\log f O_2 > -7$) at 1300°C. Specifically, they lost almost 80% of their starting Cr after 15
227 minutes. In contrast, the experiments of Norris and Wood (Norris and Wood, 2017), also
228 conducted at 1300°C and an $\log f O_2$ range of -13 to -7, provide evidence that Cr is not
229 volatile. Our experiments show no clear evidence of Cr loss, either to the loop, or by
230 volatility.
231
232   3.2. Sample preparation
233   Sample preparation for isotope measurements required a different approach between the
234 series A and B experiments. For the A series, the samples retrieved after the experiments were
235 lightly crushed in an agate mortar and pestle and the large chromite grains (>200 µm) were
236 picked from the silicate glass using a binocular stereoscope. Chromite grains were dissolved
237 in a mixture of acids (HNO_3-HCl), using Parr bombs. Despite our best efforts to separate the
238 two phases, a small amount of silicate melt often adhered to the chromite grains. As we show
239 below, this represents a negligible change to the Cr budget of the sample. The silicate melt
240 fractions were first dissolved in cold HF-HNO_3 (3:1) for 24h and then centrifuged to make
241 sure that no chromite grains were present. The samples were then dissolved in 6M HCl to
242 remove the fluorides. For the series B experiments, after crushing in an agate pestle and
243 mortar, the silicate melts were picked under a binocular microscope. The small size of the
244 chromite grains (< 15 µm) meant that it was not possible to effectively separate the chromite
245 grains from the silicate melts by hand. In order to achieve this separation, we performed a
246 sequential leaching of chromite rich sample splits. To this end, the samples were dissolved in
247 cold diluted (3M) HF for 24h. Following this, the samples were then centrifuged for 10 min at
248 3000 rpm and the supernatant was removed and discarded. The samples were then rinsed with
249 de-ionised water and centrifuged again. The isolated chromite grains were dissolved in acid
250 mixtures (HNO_3-HCl).

251   For microprobe and Raman spectroscopy analyses, small pieces of each experiment,
252 containing both silicate melts and chromite grains, were picked, mounted in epoxy and
253 polished.

254   3.3. Microprobe analyses

255   A Cameca SX5 tactis microprobe and a Cameca SX100 microprobe at the Laboratoire

256   Magmas et Volcans (LMV) were used to determine major-elements composition of the

257   chromites and silicate melts. A 15 kV accelerating voltage, a 15 nA beam current, and a 1 µm

258   electron beam were used. Standards used to calibrate the instrument were Al on Al_2O_3, Mg on

259   MgO, Na on albite, Ti and Mn on $MnTiO_3$, Ca and Si on wollastonite, Fe on Fe_2O_3 and Cr on

260   Cr_2O_3. Cr#, Fe^{3+}# and Mg# presented in this study have been calculated from EPMA analyses

261   by assuming ideal stoichiometry of the spinel phase. Fe^{3+}# and Mg# were calculated by

262   assigning Fe cations either as ferric or ferrous ions to balance negative charge (Stormer 1983).

263   Previous studies have shown that Fe^{3+}/Fe_{TOT} determination using EPMA analyses only, can

264   be affected by large analytical uncertainties (e.g. Wood and Virgo, 1989). Wood and Virgo

265   (1989) provided a robust methodology to correct for this effect using Mössbauer calibrated

266   standards. This technique has been widely used to correct EPMA analyses (e.g. Parkinson and

267   Pearce 1998). Recently, Davis et al. (2017) confirmed that the correction improves accuracy

268   and precision of Fe^{3+}/Fe_{TOT} values if the analysed chromite lies on the mantellic spinel MgO-

269   Cr# correlation. In this study, we have analysed Mössbauer calibrated chromite standards to

270   assess the accuracy of our EMPA methodology (supplementary material). We found that the

271   Fe^{3+}/Fe_{TOT} ratios obtained with our EPMA measurements are in agreement with Mössbauer

272   Fe^{3+}/Fe_{TOT} ratios obtained for the same samples (Wood and Virgo, 1989, Ionov and Wood

273   1992), which suggests that no correction is needed. Using the standard data, we have

274   determined the analytical uncertainty (2 s.d.) associated with Mg#, Cr# and Fe^{3+}#

275   calculations (± 0.013, ± 0.010 and ± 0.005, respectively).

276   3.4. Chromium isotope measurements

277   Protocols for the separation of Cr from silicate matrices have been previously published

278   (e.g. Trinquier et al. 2008; Bonnand et al. 2016a). Only a brief summary is given here:

279   Aliquots of ~2 µg of chromium of the solutions were spiked with the requisite amount of

280   ^{50}Cr-^{54}Cr double spike (Bonnand et al. 2011). The solutions were dried down and taken up in

281   6M HCl to ensure isotopic equilibrium between the samples and the spike. The protocol used

282   to separate the Cr fraction from the matrix is a two-column procedure (Bonnand et al. 2016a).

283   The first column is designed to remove the major cations while the second column removes

284   the few remaining isobaric interferences, such as Ti. The isotopic measurements were

285   performed on a ThermoFisher Triton TIMS at the University of Oxford and at the LMV.

286   Typical Cr isotope measurements consisted of 54 blocks of 10 cycles. The gains were

287   measured daily and the baselines (30 s) were measured before each block. The amplifier

288   rotation was used to cancel out the gain differences between each Faraday cup. The

289   reproducibility obtained for the JP-1 reference material over the course of this study is $\delta^{53}Cr$ =

290   -0.108 ± 0.014 ‰ (2 s.d., n = 8) in agreement with previous measurements (Bonnand et al.

291   2016a, Li et al. 2016, Zhu et al. 2018).

292

293   4. Results

294   4.1. Times series

295   The chemical compositions of the silicate melts in the time series experiments do not vary

296   except for Cr. The Cr concentration evolves from 0.02 ± 0.03 wt. % after 2 hours to 0.18

297   ±0.02 wt. % after 120 and 168 hours (Fig. 2). The Cr isotopic compositions (expressed as

298    $\delta^{53}Cr$, relative to NIST SRM 979) of the silicate melts of the time series experiments evolve

299   from -0.167 ± 0.012 ‰ after 24 h to -0.138 ± 0.012 ‰ after 168 h (Fig. 2).

300   4.2. Silicate melt chemical compositions

301   4.2.1. Series A

302   The chemical compositions of the silicate melts of the series A experiments are reported in

303   Table 3. Overall, the variations in major element composition are minor with the exception of

304   FeO in the more reduced experiment (exp A1). The SiO_2, Al_2O_3, MgO and CaO

305   concentrations in the silicate melts are 47.2, 15.4, 11.7 and 17.6 wt. %, respectively. The Cr

306   concentration (Cr_2O_3) in the silicate melts vary from 0.81 to 0.09 wt. %. The Cr

307   concentrations in the silicate melts increase with decreasing oxygen fugacity (Fig. 3).

308   4.2.2. Series B

309   The chemical compositions of the silicate melts of the series B experiments are reported in

310   Table 3. There is no variation within the three experiments for all major elements except FeO

311   with exp B1 depleted in FeO compared to exp B2 and B3. The SiO_2, Al_2O_3, MgO and CaO

312   concentrations in the silicate melts are 47.2, 15.2, 11.5 and 18.0 wt. %, respectively. The Cr

313   concentration (Cr_2O_3) in the silicate melts vary from 0.10 ± 0.03 to 0.30 ± 0.06 wt. %. The Cr

314   concentrations in the silicate melts increase with decreasing oxygen fugacity (Fig. 3).

315   4.3. Chromite chemical composition

316   4.3.1. Series A

317   The chemical compositions of the chromite grains in the series A experiments are

318   extremely variable (Figs. 4 and S2). Based on chemical compositions, the series A

319   experiments can be divided into two groups of experiments with similar behaviour. The first

320   group of experiments is composed of exp. A1 to A5 and were performed at $\log fO_2 < -6$. The

321   chromite grains are chemically heterogeneous in Mg#, Fe^{3+}# and Cr#. Experiments A1 and

322   A2 ($log fO_2$ –11.9, and –9.6, respectively) are strongly zoned with clear dissolution-

323   reprecipitation textures (Fig. S3). The newly crystallised material at the rim of the crystal is

324   up to 50 microns thick. Experiment A3 ($log fO_2$ –8.3) has a thin dark rim characterised by a

325   depletion in Fe and enrichments in Cr and Al without obvious dissolution-reprecipitation

326   textures. For the chromites of the first group of samples (A1 to A5), the rims have higher Mg#

327   values and lower Fe^{3+}# and Cr# values compared to the core compositions. The increase in

328   Mg# and decrease in Fe^{3+}# and Cr# values, across experiments, are correlated with oxygen

329   fugacity. As fO_2 decreases, Fe^{3+}# and Cr# decrease.

330   The second group of experiments is composed of the two most oxidised experiments A6

331   and A7 ($log fO_2$ –5.8, and –3.9, respectively). Their chromite grains are chemically

332   homogeneous in Mg# but heterogeneous in Fe^{3+}# with the rims enriched in Fe^{3+} and depleted

333   in Cr compared to the cores (Table 4). Interestingly, A6 and A7 chromites are enriched in Mg

334   relative to Fe^{2+} compared to the starting material compositions (Fig. 4). Overall, all series-A

335   experiments show covariation between $log\, fO_2$ and Cr# (and Fe^{3+}#) in the rims of the

336   chromite grains (Fig. 5).

337   4.3.2. Series B

338   In this experimental series, chromite grains are euhedral and up to 20 microns in size (Fig.

339   S4). The chemical composition of chromite grains crystallised in the series B experiments are

340   highly heterogeneous (Table 4 and Fig. 6). The three experiments have Mg# values ranging

341   from 0.67 to 0.79. The Fe^{3+}# and Cr# vary from 0 to 0.09 and 0.47 to 0.84, respectively. The

342   core of the bigger chromite grains have generally lower Mg# and Fe^{3+}# and higher Cr# than

343   their rims or the small chromite grains. Differences between B experiments can also be

344   observed, for example, the small (i.e. rims) chromite grains in experiments B1 have

345   systematically lower Fe^{3+}# and Mg# compared to B3 experiment (Fig. 5).

346

347   4.4. Chromium isotopic compositions

348   The Cr isotopic compositions of all silicate melts and chromite grains are given in Table 5.

349   For the silicate melts in series A and B experiments, the $\delta^{53}Cr$ values range from -0.449 $\pm$

350   0.014 to -0.117 $\pm$ 0.014 ‰ and from -0.437 $\pm$ 0.014 to -0.240 $\pm$ 0.014 ‰, respectively. The

351   chromites of the series A experiments have an average $\delta^{53}Cr$ value of -0.108 $\pm$ 0.014 ‰ (2

352   s.d., n = 7) within error of the chromite grain added to the starting material ($\delta^{53}Cr$ = -0.105 $\pm$

353   0.014 ‰). The starting material used in the series B experiments has a δ^{53}Cr value -0.060 ±

354   0.014 ‰. The chromites from the series B experiments are more heterogeneous with δ^{53}Cr

355   values ranging from 0.063 ± 0.014 to 0.150 ± 0.014 ‰.

356

357   5. Discussion

358   5.1. Chemical and isotopic evolution during the times series experiments

359   The results presented in this study show that the chemical and isotopic compositions of

360   the silicate melts in our experiments vary through time and depend on oxygen fugacity.

361   During the time series experiments the silicate melt compositions are invariant for all the

362   major elements but Cr concentrations vary (Fig. 2). In these experiments, the initial Cr

363   concentration in the melt is ~0 and it gradually increases from ~50 µg g^{-1} after 2 h to 1200 µg

364   g^{-1} after 120 h, as expected from dissolution of the chromite grains into the silicate melts. The

365   fact that the Cr concentration in the melt reaches a plateau after 120 h suggests that the Cr

366   saturation concentration in the melt has been reached, which at 1300 ℃ and log$f$O$_2$ = -8.6, is

367   approximately 1200 µg g^{-1}.

368   The Cr isotopic compositions of the silicate melts also evolve with time. After 2 hours, the

369   δ^{53}Cr value in the melt is -0.251 ‰ and it rapidly evolves to heavier values after 24 h (-0.167

370   ‰), reaching a plateau after 120 h (-0.143 ‰, Fig. 2). The dissolution of chromite into the

371   silicate melts seems to be driven by a kinetic reaction. Indeed, the first Cr going into the melts

372   is isotopically light compared to the chromite starting material and it evolves toward heavier

373   values with time (Fig. 2). As with the Cr concentrations, it seems that the isotopic

374   composition of the melt reaches steady state after 120-168 h. Due to the slow diffusion rate of

375   Cr^{3+} in the chromite and the resulting zoning observed in chromite of the series A

376   experiments, it is impossible to argue for full isotopic equilibrium in the experimental charge.

377   However, the plateau observed in the time series experiments suggests that the Cr isotopic

378   compositions of the silicate melts are at local equilibrium with the rims of the chromite and

379   we argue that the silicate melts approach Cr isotopic composition equilibrium after 120 h. We

380   therefore decided to run our other experiments for 168 h in order to reach the Cr saturation

381   concentration in the silicate melts and to approach isotopic equilibrium.

382   5.2. Chemical evolution of the silicate melt compositions

383   The chemical composition of the silicate melts in individual experiments and between the

384   experiments of the series A and B are homogeneous, except for Cr. In Figure 3, the Cr

385   concentration in both series of experiments are plotted against oxygen fugacity. The Cr

386 concentration in the melt increases with decreasing oxygen fugacity (Fig. 3). The two series

387 of experiments lie on the same solubility curve highlighting that, in both cases, the Cr

388 concentration of the melt has closely approached equilibrium with the chromite. Importantly,

389 the increase in Cr solubility in the silicate melts with decreasing fO_2 is in agreement with

390 previous studies that had already shown that Cr is more soluble in silicate melts under

391 reducing conditions (Fig. 2, Roeder and Reynolds 1991; Hanson and Jones 1998).

392 In a silicate melt, chromium occupies two principal oxidation states, Cr^{2+} and Cr^{3+}. Cr^{2+} is

393 absent from room-temperature silicate glasses due to the oxidation of Cr ($Fe^{3+} + Cr^{2+} \rightarrow Fe^{2+}$

394 $+ Cr^{3+}$) during quenching (Berry et al. 2006). This makes it impossible to measure the

395 Cr^{2+}/Cr^{3+} ratio in our silicate glasses. Hanson and Jones (1998) have proposed a method to

396 calculate the Cr^{2+}/Cr^{3+} ratios in silicate melts in the presence of spinel. The main assumption

397 in this method is that i) at the Ni-NiO oxygen buffer, Cr is only present in Cr^{3+}, and ii) that the

398 Cr^{3+} concentration in the melt is independent of fO_2 (Hanson and Jones 1998). The latter

399 assumption is based on the fact that, in the presence of spinel, the activity of Cr^{3+} ($aCrO_{1.5}$)

400 remains constant and does not vary with fO_2. In order to calculate the Cr^{2+}/Cr^{3+} ratio in our

401 silicate melts, we used the following equation:

402 $$Cr^{2+}/Cr^{3+} = (Cr_{melt} - Cr_{oxy}) / Cr_{oxy}$$

403 where Cr_{melt} and Cr_{oxy} are the Cr concentrations in a given experiment and in the most

404 oxidised experiment, respectively. The similarity in composition and experimental conditions

405 between the A and B series means that for the Cr^{2+}/Cr^{3+} calculation, we assume that the Cr^{3+}

406 concentration in our experiments is the average Cr concentration in the experiments

407 performed above the Ni-NiO buffer (A6, A7 and B3). In Figure 7, we report the

408 $log(Cr^{2+}/Cr^{3+})$ versus the log of oxygen fugacity for our series of experiments. We obtain a

409 slope of -0.25 ± 0.01 (series A) and -0.27 ± 0.01 (series B) close to the theoretical slope of

410 -0.25 expected for a redox reaction involving a one electron exchange. This is strong

411 evidence that the increase in Cr solubility in our experiments under reducing conditions is

412 controlled by the difference in solubility between Cr^{3+} and Cr^{2+} in silicate melts. This

413 conclusion is in agreement with previous studies on this topic (e.g. Hanson and Jones 1998).

414 Together with Cr, Fe is another redox sensitive element and the Fe^{3+}/Fe_{TOT} in the silicate

415 melt is also expected to vary with fO_2. We have calculated the Fe^{3+}/Fe_{TOT} ratio in our silicate

416 melts using the calibration given in O'Neill et al. (2018). The results of this calculation are

417 shown in Figure 7b. As expected, given the temperature and the redox conditions in which we

13

418 performed our experiments the Fe^{3+}/Fe_{TOT} ratio varies greatly in our silicate melts from 0.02

419 to 0.45 (Table 3). The amount of Fe^{3+} in the melt varies less than the Cr^{3+}/Cr_{TOT} ratio

420 calculated above because the oxidation reaction for Fe happens at higher fO$_2$ than that of Cr.

421

422   5.3. Chromite chemical evolution

423 The chromite grains analysed in this study are heterogeneous. The large variations in

424 chemical composition, illustrated by the zoning observed in the chromite from the series A

425 experiments, clearly indicate that the cores of the chromite grains are not at equilibrium with

426 the silicate melts. This can be easily explained by the slow diffusion rate of Cr^{3+} in chromite

427 (Suzuki et al. 2008). However, several systematics in the chromite zoning can be identified

428 (Fig. 4 and S1). For the two most oxidised experiments (exp A6 and A7), the Mg# is

429 homogeneous and higher than the Mg# in the starting material. This observation indicates

430 that, under oxidising conditions, Mg^{2+} and Fe^{2+} diffuse relatively fast and have sufficient time

431 to equilibrate with the melt. In the same experiments, the Fe^{3+}# is higher in the rim than in the

432 cores (Fig. 4). This suggests that the original chromite grain was depleted in Fe^{3+} compared to

433 the chromite at equilibrium with the silicate melts. The trends observed can be explained by

434 diffusion of Fe^{3+} from the melt together with diffusion of Al and Cr from the chromite to the

435 melt.

436 In the more reduced experiments, the chromite grains are zoned in Mg#, Fe^{3+}# and Cr#.

437 The Mg# is higher in the rims than in the cores (Fig. 4), indicating that the starting material

438 was Fe^{2+} rich compared to the chromite at equilibrium with the silicate melts at different fO$_2$.

439 This indicates that Fe^{2+} diffuses out of the chromite grain even at low fO$_2$ but the diffusion

440 rate of Mg^{2+} and Fe^{2+} in the chromite is slower under more reducing conditions. The Mg# in

441 the rims does not correlate with fO$_2$. The Fe^{3+}# and Cr# are both lower in the rims than in the

442 cores which suggests that the chromite grains are losing Fe and Cr to the melt and/or gaining

443 Al from the melt. This is consistent with a decrease in Fe^{3+}/Fe_{TOT} and Cr^{3+}/Cr_{TOT} in the

444 silicate melts described in the section above. As for the most oxidised experiments, the cores

445 of chromite are not at equilibrium with the silicate melts.

446 In Figure 4, all chromite data are reported and general trends can be easily seen. First, there

447 is a clear fO$_2$ control on the rate of diffusion of Fe^{2+} in the chromite grains. Indeed, although

448 all rims tend to have higher Mg# values compared to the starting material, it is clearly the

449 most oxidised experiments that have the highest Mg#. Considering Fe^{3+}# and Cr#, the rims

450   values are also extremely variable and, overall, the oxidised experiments have higher $Fe^{3+}\#$

451   values compared to the more reduced experiments. The rim chemical compositions are

452   strongly controlled by fO_2 and this is shown in Figure 5. There is a positive correlation

453   between Cr# and $Fe^{3+}\#$ in the rim compositions and fO_2. The most reduced experiments have

454   rim Cr# and $Fe^{3+}\#$ compositions of 0.5 and 0, respectively. The more oxidised experiments

455   have rim compositions of 0.7 and 0.12. This clearly shows that the composition of the

456   chromite grains in our experiments is controlled by fO_2. Under reducing conditions, Fe^{3+} and

457   Cr^{3+} are lost from the initial chromite. Under more oxidised conditions, Fe^{3+} becomes more

458   stable in the chromite structure and Cr is also favoured. Assuming the rim compositions are in

459   equilibrium with the silicate melts then, this indicates that the partition coefficient of Cr and

460   Fe between chromite and a silicate melt is strongly fO_2 dependent. The D_{Cr} ($D_{Cr} =$

461    $Cr_{chromite}/Cr_{melt}$) calculated between the rims and the silicate melts in the experiments series A

462   are presented in Figure 8. The D_{Cr} values vary from 55 to 570 and there is a good correlation

463   between D_{Cr} and fO_2. We also present D_{Cr3+} ($D_{Cr3+} = Cr_{chromite}/Cr^{3+}_{melt}$) using the calculations

464   presented in section 5.1. In the series A, the D_{Cr3+} increases with fO_2 (from $\log fO_2 = -12$ to

465    $\log fO_2 = -6$) and then there is a break with smaller D_{Cr3+} values at $\log fO_2 > -6$ (Fig. 8). This

466   suggests that Cr^{3+} becomes less compatible in chromite under oxidising conditions.

467   In the series B experiments, the chromite grains are also extremely variable. In this study,

468   we have systematically analysed the large and small chromite grains (Fig. 6). Both core and

469   rims were analysed in the large chromite (> 15 µm). The data are presented in Figure 6. The

470   core compositions in all experiments have high Cr_2O_3 concentrations and low Mg#. The rim

471   and small chromites compositions have lower Cr_2O_3 concentrations and higher Mg# (Table

472   4). This suggests that during fractional crystallisation the chemical composition of the

473   chromite strongly depends on the silicate melt chemical composition. Indeed, the decrease in

474   Cr_2O_3 content in the chromite is controlled by the concentration in the silicate melts while

475   crystallisation proceeds. Interestingly, the Fe^{3+} content in the chromite also evolves with

476   fractional crystallisation but is strongly dependent on the redox conditions of the experiments.

477   This is also true for Cr content but the variations are smaller. Our experiments show that the

478   redox conditions during the experiments control the chemical composition of the crystallising

479   phases. This is best observed in Figure 5, where the $Fe^{3+}\#$ and Cr# of the small chromite

480   grains are plotted versus fO_2. The Fe^{3+} content of the chromite increases with increasing fO_2

481   as observed for the series A chromite. The fact that the chromite grains are chemically

482   heterogeneous indicates that they are not all in equilibrium with the silicate melts. The slow

483 diffusion of Fe^{3+} and Cr in the chromite lattice means that there is no chemical re-

484 equilibration after the chromites have crystallised out of the silicate melts. This observation

485 provides evidence that the small chromites and rims of the larger grains are more likely to

486 represent the chemical composition of the chromite at equilibrium with the silicate melts. As

487 with the series A experiments, the Cr contents of the small chromite grains were used to

488 calculate partition coefficients (D_{Cr}) which vary from 150 to 390 and are positively correlated

489 with fO_2 (Fig. 8). The partition coefficient values are very similar to the values obtained with

490 the series A experiments. The D_{Cr3+} for the series B experiments are slightly negatively

491 correlated with fO_2 which confirms that under oxidising conditions Cr^{3+} becomes less

492 compatible in chromite. The Fe^{3+}# in the small chromite grains most likely at equilibrium

493 with the silicate melts is correlated with fO_2 (Figure 5). This correlation is very similar to the

494 correlation shown above for the series A experiments. The similarity in Cr concentration, D_{Cr}

495 and Fe^{3+}# of small chromite obtained for the series B experiments and the rims of series A

496 chromite, suggests that although there is not chemical equilibrium between the silicate melts

497 and the entire chromite grains, the rims of the chromite grains are at local equilibrium with the

498 silicate melts.

499   5.4. Chromium isotope variations
500   5.4.1. Chromites

501   The Cr isotopic compositions of the chromites in the series A experiments show little

502 variation. This can be explained by the lack of equilibration between the cores of the chromite

503 grains and the silicate melts, due in large part to the grain size. In this study, the chromites

504 were handpicked from experimental facilitating analysis of single grains. The fact that the

505 reaction rims in the chromite grain are small (relative to the size of the grain) means that Cr

506 isotope measurements of chromite is dominated by the composition of the core. Thus, it is

507 unsurprising that the Cr isotopic compositions of the chromite grains are within error of that

508 of the starting material. This suggests that these compositions are not at equilibrium with the

509 silicate melts and are not discussed further in this manuscript.

510   5.4.2. Series A

511   The Cr isotopic compositions of the silicate melts in the series A experiments are lighter

512 than the Cr isotopic composition of the initial chromite added. This suggests that chromite is

513 isotopically heavier than silicate melts, an observation that agrees with both ab-initio

514 calculation and inferences based on lunar and terrestrial samples (Schoenberg et al. 2008,

515 Moynier et al. 2011, Shen et al. 2018, Bonnand et al. 2016, Bonnand et al. 2020, Farkas et al.

516 2013). In the series A experiments, the Cr isotopic compositions of the silicate melts can be

517 divided into two domains: experiments at $\log fO_2$ above -6, silicate melts have $\delta^{53}Cr$ of

518 approximately -0.45 ‰, while experiments run at $\log fO_2$ below -6, silicate melts have $\delta^{53}Cr$

519 of approximately -0.15 ‰ (Fig. 9). Additionally, for those experiments run at $\log fO_2$ lower

520 than -6, the Cr isotopic composition of the silicate melts is negatively correlated with the

521 redox conditions and the Cr^{3+}/Cr_{TOT} of the silicate melts (Fig. 10). In these experiments, the

522 Cr isotopic composition in the melts decreases from $\delta^{53}Cr=-0.12$‰ to $\delta^{53}Cr=-0.15$‰ as

523 $\log fO_2$ increases from -12 to -7.

524   It is possible that the observed variations are controlled by the redox conditions. In this

525 case, the change in isotopic composition could be due to the fact that, at equilibrium, Cr^{2+} and

526 Cr^{3+} in the melts have different isotopic compositions. If this is the case, then we would

527 expect to see $\delta^{53}Cr$ varying with the Cr^{3+}/Cr_{TOT} ratio (and fO_2). It is important to note,

528 however, that the $\delta^{53}Cr$ of silicate melts is lighter with increasing Cr^{3+}/Cr_{TOT}, implying that

529 Cr^{3+} is lighter than Cr^{2+}. Ab-initio calculations suggest the opposite; Cr^{3+} is assumed to be

530 isotopically heavy compared to Cr^{2+} ($\Delta Cr^{3+}-Cr^{2+} = 0.35*10^6/T^2$, Moynier et al. 2011). In

531 summary, the Cr isotopic composition of silicate melts in contact with magnesiochromite

532 depends on oxygen fugacity. Under reducing conditions, the Cr isotopic composition of the

533 silicate melt is isotopically heavier than silicate melts produced at higher fO_2. This suggests

534 that Cr isotopes could be a powerful tool to study redox conditions in high temperature

535 environments.

536   Importantly, the two most oxidised experiments have very light Cr isotopic compositions,

537 which could reflect diverse causes. The small Cr concentration in the silicate melts indicates

538 that the amount of chromite dissolving into the melt in oxidised conditions is small and could

539 potentially limit the attainment of local equilibrium between chromite and the silicate melts. It

540 is important to note, however, that the chromite grains in those experiments are the least

541 zoned (although different from the starting composition) which suggests that they have

542 reached equilibrium more rapidly than those under reducing conditions. It is surprising that in

543 the most oxidised conditions, where all Cr is believed to be Cr^{3+}, that the silicate melts exhibit

544 the largest isotopic shifts. Although this observation is consistent with the observation made

545 for more reduced experiments (melts lighter than chromite), the shift in isotopic composition

546 is large, and seemingly abrupt.

547   Three main mechanisms can be put forward to explain these light values. The Cr isotopic

548 compositions in the silicate melts are controlled by (i) the chemical composition and the

549 structure of the silicate melt, (ii) the chemical composition and the structure of the chromite

550 grains and (iii) the isotopic fractionation during volatilisation of Cr under high fO_2 conditions.

551 As explained above, depending on the Fe^{3+}/Fe_{TOT} ratio in silicate melt, the Fe^{3+} coordination

552 in the silicate melts vary. In this study, the two most oxidised experiments have Fe^{3+}/Fe_{TOT}

553 ratio > 0.3 and are also characterised by Raman spectra that could indicate a change in

554 coordination number for Fe. There is a possibility that this change in the melt structure might

555 also affect the coordination of Cr^{3+} in the melt. The Cr isotopic shift observed at about $logfO_2$

556 $= -6$ could be the result of a change in Cr^{3+} coordination in the melt. In this case, a change of

557 Cr^{3+} coordination in the melt from VI fold to IV fold could explain the lighter Cr isotopic

558 composition in the silicate melts in oxidising conditions. This suggestion is supported by the

559 changes in the Raman spectra of both experiments performed under oxidizing conditions (Fig.

560 S5). However, it is generally thought that lower coordination number favours heavy isotopes

561 (Young et al. 2015). Alternatively, a change in Cr neighbours in the silicate melt structure

562 could also explain the shift in Cr isotopic composition. A lower force constant in the Cr-O

563 bond could indeed results in lighter Cr isotopic compositions. It is also possible that Cr may

564 be present under Cr^{6+} in the silicate melts above $logfO_2 = -6$ and this could be responsible for

565 the observed isotopic shifts. Given the fact that Cr undergoes redox changes during

566 quenching, it is very difficult to assess a change in oxidation state and in coordination

567 number.

568 The second hypothesis is that the chemical composition of the chromite grain controls the

569 observed isotopic shift. In this case, the hypothesis is that under oxidising conditions, Fe^{3+}

570 becomes more compatible in magnesiochromite resulting in a competition between Cr^{3+} and

571 Fe^{3+}. This is supported by the decrease in D_{Cr3+} with fO_2 observed in our experiments (550 to

572 450 for experiments above and below $logfO_2 = -6$, respectively). This would suggest that the

573 result of this competition would be a change in the equilibrium fractionation factor between

574 chromite and the silicate melt. In this case, the fractionation factor between chromite and

575 silicate melts is higher under oxidising conditions and would be inversely correlated with D_{Cr}.

576 Finally, it had been recently argued that Cr is volatile under oxidised conditions (Sossi et

577 al. 2019). The variations in the most oxidised experiments may be caused by loss of

578 isotopically heavy Cr during volatilisation. Our experiments are not designed to quantify the

579 volatility of Cr because the samples after the experiments are not 100% recovered which

580 inhibits mass balance calculation. It is thus difficult to assess whether volatile loss has

581 occurred. The constant flow of gas employed in our experiments means that any evaporative

582 loss will not be at isotopic equilibrium with the silicate melt. Sossi et al. (2019) reported that

583 Cr concentration decreased by ~40% at $\log fO_2 = -5.6$ in 15 minutes at 1300 °C. If

584 volatilisation were the main process controlling the Cr budget in our silicate melts, we would

585 have observed severe depletion in Cr concentration in our experiment performed at $\log fO_2 =$

586 -3.9 and for ~10,000 minutes. Since such depletion did not occur, we consider that volatile

587 loss of Cr is not a significant influence on our results.

588   5.4.3. Series B

589   In the series B experiments, the Cr isotopic measurements of the chromites were made on

590 multi-grain samples, due to the small size (< 10 µm) of the chromites precipitated from the

591 silicate melt. The HCl leaching method used in this study did not selectively sample the small

592 chromite grains but can be regarded as an average composition of chromite in each

593 experiment and not the Cr isotopic composition at equilibrium with the silicate melts.

594 Nevertheless, the Cr isotopic compositions of the chromite in the series B experiments are

595 heavy (by ~0.3 ‰) compared to the Cr isotopic composition of the starting material. This

596 suggests that during fractional crystallisation the chromites are isotopically heavy compared

597 to the silicate melts. This observation is in agreement with the Cr isotopic variations observed

598 in lunar basalt and terrestrial basalts (Bonnand et al. 2016, Bonnand et al. 2020, Shen et al.

599 2020) and also with ab-initio calculations (Moynier et al. 2011) and mineral separates data

600 where chromite is the heaviest of Cr-bearing phases (Shen et al. 2018).

601   The Cr isotopic compositions of the silicate melts in the series B experiments are

602 isotopically light compared to the starting material. Like the series A experiments, the Cr

603 isotopic composition of the melt in the more reduced experiment in series B is also heavier

604 than the isotopic composition of the silicate melts at higher fO_2 (-0.24 and -0.44 at $\log fO_2$ of

605 -10 and -6, respectively; see Fig. 9). Unfortunately, we do not have access to both the melts

606 and the chromite at complete equilibrium. In this series of experiments, the main reaction is

607 fractional crystallisation. We have modelled the Cr isotopic composition of the silicate melts

608 during fractional crystallisation using the initial Cr concentration and isotopic composition of

609 the starting silicate melts. In Figure 11, we show two fractional crystallisation models, one

610 Rayleigh fractionation model and one equilibrium fractionation model. Using this conceptual

611 framework, the isotopic fractionation measured in our experiments represents an average over

612 the entire crystallisation sequence. Two cases can be considered, one in which the isotopic

613 fractionation factor is constant during the entire crystallisation sequence; the second in which

614 it evolves during crystallisation proceeds. In the models presented in Figure 11, the Cr

isotopic compositions of the crystallising chromite is lighter than that measured for the chromite in the series B experiments (Fig. 11). This provides evidence that the fractionation factors vary during crystallisation and are averages from the start of the crystallising sequence to the end. The variation could be linked to the change in the silicate melts chemical composition but also to the change in temperature during the experiments. The results of these models show that experiments B1 and B2 can be explained by a similar ε factor, whereas the most oxidised experiment B3 clearly requires a larger isotopic fractionation between crystallising chromite and the melt. This is in agreement with the observation that under more oxidised conditions the melt is more depleted in heavy isotopes than the melts produced at lower fO_2. This shift in isotopic composition could be linked to the fact that the chemical composition of the chromite grains is controlled by fO_2. The fractionation factor is therefore linked to fO_2 and it is surprising that fractionation factors between chromite and Cr^{3+} in the melt are larger than chromite and Cr^{2+} in the melt. This is difficult to explain with ab-initio calculations because changes in valence state are supposed to lead to higher fractionation factor than changes in bonding environment (Schauble, 2004). In this case, however, it seems that bonding environment in chromite under oxidising conditions strongly favours heavy isotopes. As previously proposed for the series A experiments, the Cr isotopic shift at high fO_2 could be explained by (i) a change in bonding environment in the melts, (ii) a change in bonding environment in the crystallising chromites and (iii) Cr isotopic fractionation during Cr volatilisation under oxidising conditions.

5.5. Implications for Cr isotopes at high temperature

The results of this study can be used to make general comments on Cr isotope behaviour during igneous processes such as partial melting. Our measurements predict that during partial melting, the silicate melts will be enriched in light isotopes, and the residues will be enriched in heavy isotopes. Recent measurements of ocean island basalts (Shen et al. 2020, Bonnand et al. 2020) and in mantle peridotites (Xia et al. 2017, Shen et al. 2018, Bai et al. 2019) show that residues tend to be 0.05 ‰ heavier than products. Furthermore, the results on the time series experiments demonstrate that in non-equilibrium partial melting reactions, Cr isotope fractionations are driven by kinetic reaction and the melts are enriched in light isotopes. Non-equilibrium melting reactions in natural systems would results in enrichment in heavy isotopes in the residues as suggested by Xia et al. (2017). Importantly, our measurements were performed at 1 atmosphere and so the results of these experiments are not directly

648 transferable to natural systems. The impact of pressure on the Cr isotope behaviour should be

649 studied in order to evaluate this.

650   The isotopic variations observed in the experiments performed in this study clearly

651 highlight for the first time, the role played by oxygen fugacity in the behaviour of Cr and its

652 isotopes. It seems that fractionations between chromite and silicate melts are larger under

653 oxidising conditions and this possibly could be useful for studying redox reactions in natural

654 systems. This observation, however, is in disagreement with recent data suggesting that

655 during fractional crystallisation, the Cr isotopic fractionation is smaller under oxidising

656 conditions (Shen et al. 2020, Bonnand et al. 2020). Indeed, the observed variations in

657 terrestrial samples for some OIBs can be modelled with fractionation factors ($\Delta^{53}Cr_{crystal\text{-}melts}$)

658 ranging from −0.005 to −0.02 ‰ (Shen et al. 2020, Bonnand et al. 2020). Under more

659 reducing conditions, the fractionation factor used to model the lunar basalts variations is

660 −0.07 ‰. The dichotomy between two recent datasets of natural OIB samples and our

661 experiments suggest that either chromite is not controlling the Cr budget during fractional

662 crystallisation of OIB samples or that other physical parameters play a role in controlling Cr

663 isotope fractionation. Our study clearly shows that a better understanding of Cr isotopes

664 behaviour in high temperature systems is needed.

665

666 6. Conclusions

667

668   We have investigated the variations in chemical composition and Cr isotopic compositions

669 in both magnesiochromite and silicate melts during experiments performed under controlled

670 redox conditions. Two series of experiments were performed to study both dissolution (series

671 A) and crystallisation (series B) reactions.

672   Overall, the chemical composition of the silicate melts is relatively constant with the

673 exception of Cr. As expected, the Cr solubility in silicate melts in our experiments is

674 controlled by temperature and oxygen fugacity. We confirm that chromium becomes more

675 soluble under reducing conditions. The chemical compositions of the chromite in the

676 dissolution experiments (series A) are extremely variable as demonstrated by their zoning in

677 each experiment. The Fe^{3+}# in the rims correlates with fO_2 and this indicates that the chemical

678 composition of the chromites are controlled by fO_2. The partition coefficient of Cr between

679 chromite and silicate melts vary with fO_2; DCr is positively correlated with fO_2 and DCr^{3+} is

680 weakly negatively correlated. This indicates that Cr^{3+} becomes less compatible in chromite

681 under oxidising conditions because of the competition with Fe^{3+}. In the series B experiments,

682 the chromite grains are heterogeneous and several processes play a role in the observed

683 chemical evolution: the redox conditions, the temperature and the chemical composition of

684 the evolving silicate melts. Raman spectroscopy was used to analyse both silicate melts

685 (series A and B) and in chromite (series B only). In summary, the Raman spectra are strongly

686 influenced by the presence of Fe^{3+} in both the melts and the chromite grains. The changes in

687 the Raman spectra do not allow us to definitively show a change in Fe^{3+} coordination in the

688 silicate melts. However, the differences in Raman spectra clearly indicate that the experiments

689 performed under oxidising conditions are structurally distinct from the experiments performed

690 under reducing conditions.

691   The Cr isotopic compositions measured in the silicate melts in both series A and B

692 experiments are strongly influenced by oxygen fugacity. The Cr isotopic composition of the

693 silicate melts in the experiments from the series A group performed at $\log fO_2 < -6$ are

694 correlated with fO_2. This suggests that Cr isotopes is a powerful tool to study changes in redox

695 conditions in high temperature processes. The Cr isotopic composition of the silicate

696 performed under more oxidising conditions are isotopically much lighter. Two main factors

697 (not mutually exclusive) are proposed to explain such variations: (i) a change in Cr bonding

698 environment in the silicate melt (ii) a change in Cr bonding environment in the chromite.

699 More work is needed to definitively determine the factors that control the isotopic behaviour

700 of Cr in silicate melts. Finally, the Cr isotopic composition for the series B experiments

701 indicate that Cr isotopes are fractionated during fractional crystallisation of magnesiochromite

702 from silicate melts. As also shown in the series A experiments, it seems that the fractionation

703 factor is higher under oxidised conditions. Our work also shows that it is likely that the

704 fractionation factor during fractional crystallisation varies with the chemical composition of

705 the chromites, the chemical composition of the silicate melts and temperature. These factors,

706 in addition to the fO_2, likely play a major role in controlling Cr isotope behaviour in igneous

707 processes.

708

709

710

711

712

713

714

715

716

717

718

719

726

727   Declaration of competing interest:

728   We have no competing financial interests or personal relationship that could have appeared to

729   influence the work reported in this paper.

730

731

732

733

734

735

736

737

738

739

References:

Bai Y., Su B.X., Xiao Y., Chen C., Cui M.M., He X.Q., Qin L.P., Charlier B., (2019) Diffusion-driven chromium isotope fractionation in ultramafic cumulate minerals: Elemental and isotopic evidence from the Stillwater Complex. *Geochim. Cosmochim. Acta* **263**, 167–181. https://doi.org/10.1016/j.gca.2019.07.052

Berry A. J. and O'Neill H. S. C., (2004) A XANES determination of the oxidation state of chromium in silicate glasses. *Am. Mineral.* **89**, 790–798.

Berry A. J., O'Neill H. S. C., Scott D. R., Foran G. J., Shelley J. M. G., (2006) The effect of composition on Cr2+/Cr3+ in silicate melts. *Am. Mineral.* **91**, 1901–1908. https://doi.org/10.2138/am.2006.2097

Biagioni C. and Pasero M. (2014) The systematics of the spinel-type minerals: An overview *Am. Mineral.* **99**, 1254–1264.

Blundy J. and Wood B. (2003) Partitioning of trace elements between crystals and melts. *Earth Planet. Sci. Lett.* **210**, 383–397. https://doi.org/10.1016/S0012-821X(03)00129-8

Bodinier J. L. and Godard M. (2013) Orogenic, Ophiolitic, and Abyssal Peridotites, 3rd ed, *Treatise on Geochemistry*: Second Edition. Elsevier Ltd. https://doi.org/10.1016/B978-0-08-095975-7.00204-7

Bonnand P. and Halliday A.N. (2018) Oxidized conditions in iron meteorite parent bodies. *Nat. Geosci.* **11**, 401-405. https://doi.org/10.1038/s41561-018-0128-2

Bonnand P., Parkinson I. J., James R. H., Karjalainen A.-M., Fehr M. A. (2011) Accurate and precise determination of stable Cr isotope compositions in carbonates by double spike MC-ICP-MS. *J. Anal. At. Spectrom.* **26**, 528–535. https://doi.org/10.1039/c0ja00167h

Bonnand P., Parkinson I. J., Anand M. (2016a) Mass dependent fractionation of stable chromium isotopes in mare basalts: Implications for the formation and the differentiation of the Moon. *Geochim. Cosmochim. Acta* **175**, 208–221. https://doi.org/10.1016/j.gca.2015.11.041

Bonnand P., Williams H. M., Parkinson I. J., Wood B. J., Halliday A. N. (2016b) Stable chromium isotopic composition of meteorites and metal-silicate experiments: Implications for fractionation during core formation. *Earth Planet. Sci. Lett.* **435**, 14–21. https://doi.org/10.1016/j.epsl.2015.11.026

Bonnand P., Doucelance R., Boyet M., Bachèlery P., Bosq C., Auclair D., Schiano P., (2020) The influence of igneous processes on the chromium isotopic compositions of terrestrial basalts. *Earth Planet. Sci. Lett.* **532**, 116028. https://doi.org/10.1016/j.epsl.2019.116028

Bourdon B., Roskosz M., Hin R. C. (2018) Isotope tracers of core formation. *Earth-Science Rev.* **181**, 61–81. https://doi.org/10.1016/j.earscirev.2018.04.006

Davis F. A., Cottrell E., Birner S. K., Warren J. M., Lopez O. G. (2017) Revisiting the electron microprobe method of spinel-olivine-orthopyroxene oxybarometry applied to spinel peridotites. *Am. Mineral.* **102**, 421–435. https://doi.org/10.2138/am-2017-5823

Dick H. J. B. and Bullen T., (1984) Chromian spinel as a petrogenetic indicator in abyssal and alpine-type peridotites and spatially associated lavas. *Contrib. to Mineral. Petrol.* **86**, 54–76. https://doi.org/10.1007/BF00373711

Farkas J., Chrastny V., Novak M., Cadkova E., Pasava J., Chakrabarti R., Jacobsen S. B., Ackerman L., Bullen T. D. (2013) Chromium isotope variations (delta Cr-53/52) in mantle-derived sources and their weathering products: Implications for environmental studies and the evolution of delta Cr-53/52

781   in the Earth's mantle over geologic time. *Geochim. Cosmochim. Acta* **123**, 74–92.
782   https://doi.org/10.1016/j.gca.2013.08.016

783   Frost D. J. and McCammon C. A. (2008). The Redox State of Earth's Mantle. *Annu. Rev. Earth*
784   *Planet. Sci.* **36**, 389–420. https://doi.org/10.1146/annurev.earth.36.031207.124322

785   Hanson B. and Jones J. H. (1998). The systematics of Cr3+ and Cr2+ partitioning between olivine and
786   liquid in the presence of spinel. *Am. Mineral.* **83**, 669–684.

787   Horn I., Foley S. F., Jackson S. E., Jenner G. A. (1994). Experimentally determined partitioning of
788   high field strength- and selected transition elements between spinel and basaltic melt. *Chem. Geol.*
789   **117**, 193–218. https://doi.org/10.1016/0009-2541(94)90128-7

790   Huang J., Hao J., Huang F., Sverjensky D.A. (2019), Mobility of chromium in high temperature
791   crustal and upper mantle fluids; Geochemical Perspective Letters. 2019, Vol, 12, p. 1-6.

792   Ionov D. A. and Wood B. J. (1992) The oxidation state of subcontinental mantle: oxygen
793   thermobarometry of mantle xenoliths from central Asia. *Contrib. to Mineral. Petrol.* **111**, 179–193.
794   https://doi.org/10.1007/BF00348950

795   Keppler H. (1992) Crystal field spectra and geochemistry of transition metal ions in silicate melts and
796   glasses. *Am. Mineral.* **77**, 62–75.

797   Khedim H., Podor R., Rapin C., Vilasi M. (2008) Redox-control solubility of chromium oxide in soda-
798   silicate melts. *J. Am. Ceram. Soc.* **91**, 3571–3579. https://doi.org/10.1111/j.1551-2916.2008.02692.x

799   Li C. F., Feng L. J., Wang X. C., Chu Z. Y., Guo J. H., Wilde S. A, (2016) Precise measurement of Cr
800   isotope ratios using a highly sensitive Nb2O5 emitter by thermal ionization mass spectrometry and an
801   improved procedure for separating Cr from geological materials. *J. Anal. At. Spectrom.* 31, 2375–
802   2383. https://doi.org/10.1039/c6ja00265j

803   Li J.-P., O'Neill H., Seifert F. (1995). Subsolidus Phase Relations in the System MgO-SiO 2-Ci^O in
804   Equilibrium with Metallic Cr, and their Significance for the Petrochemistry of Chromium Subsolidus
805   phase relations have been determined in the systems. *J. Petrol.* **36**, 107–133.

806   Liu, X. and O'Neill, H. S. C. (2004) The effect of Cr2O3 on the partial melting of spinel
807   lherzolite in the system CaO-MgO-Al2O3-SiO2-Cr2O3 at 1.1 GPa. *J. Petrol.* **45**, 2261–2286.
808   https://doi .org /10 .1093 /petrology /egh055.

809   Maclennan J., McKenzie D., Hilton F., Gronvold K., Shimizu N. (2003) Geochemical variability in a
810   single flow from northern Iceland. *J. Geophys. Res.* Earth **108**. https://doi.org/10.1029/2000JB000142

811   McKenzie, D. and O'Nions, R. K. (1995). The source regions of ocean island basalts. *J.*
812   *Petrol.* **36**, 133–159. https://doi .org /10 .1093 /petrology /36 .1

813   Moynier F., Yin Q.-Z., Schauble E. (2011) Isotopic Evidence of Cr Partitioning into Earth's Core.
814   *Science* **331**, 1417–1420. https://doi.org/10.1126/science.1199597

815   Murck B. W. and Campbell I. H. (1986) The effects of temperature, oxygen fugacity and melt
816   composition on the behaviour of chromium in basic and ultrabasic melts. *Geochim. Cosmochim. Acta*
817   **50**, 1871–1887. https://doi.org/10.1016/0016-7037(86)90245-0

818   Naldrett A. J., Wilson A., Kinnaird J., Chunnett G. (2009) PGE tenor and metal ratios within and
819   below the Merensky Reef, Bushveld Complex: Implications for its genesis. *J. Petrol.* **50**, 625–659.
820   https://doi.org/10.1093/petrology/egp015

821   Nebel O., Campbell I. H., Sossi P. A., Van Kranendonk M. J. (2014) Hafnium and iron isotopes in
822   early Archean komatiites record a plume-driven convection cycle in the Hadean Earth. *Earth Planet.*
823   *Sci. Lett.* **397**, 111–120. https://doi.org/10.1016/j.epsl.2014.04.028

824   Nielsen R. L. and Beard J. S. (2000) Magnetite – melt HFSE partitioning. *Chem. Geol.* **164**, 21–34.

825   Nielsen R. L., Forsythe L. M., Gallahan W. E., Fisk M. R. (1994) Major- and trace-element magnetite-
826   melt equilibria. *Chem. Geol.* **117**, 167–191.

827   Norris C. A., Wood B. J. (2017) Earth's volatile contents established by melting and vaporization.
828   *Nature* **549**, 507–510. https://doi.org/10.1038/nature23645

829   O'Neill H. S. C., Berry A. J., Mallmann G. (2018) The oxidation state of iron in Mid-Ocean Ridge
830   Basaltic (MORB) glasses: Implications for their petrogenesis and oxygen fugacities. *Earth Planet. Sci.*
831   *Lett.* **504**, 152–162. https://doi.org/10.1016/j.epsl.2018.10.002

832   Parkinson I. J. and Pearce J. A. (1998) Peridotites from the Izu-Bonin-Mariana forearc (ODP Leg
833   125): evidence for mantle melting and melt-mantle interaction in a supra-subduction zone setting. *J.*
834   *Petrol.* **39**, 1577–1618. https://doi.org/10.1093/petroj/39.9.1577

835   Roeder P. L. and Reynolds I. (1991) Crystallisation of chromite and chromium solubility in basaltic
836   melts. *J. Petrol.* **32**, 909–934. https://doi.org/10.1093/petrology/32.5.909

837   Schauble E. A. (2004) Applying Stable Isotope Fractionation Theory to New Systems. Reviews in
838   Mineralogy & Geochemistry, **55**, 65-111.

839   Schoenberg R., Merdian A., Holmden C., Kleinhanns I. C., Hassler K., Wille M., Reitter E. (2016)
840   The stable Cr isotopic compositions of chondrites and silicate planetary reservoirs. *Geochim.*
841   *Cosmochim. Acta* **183**, 14–30. https://doi.org/10.1016/j.gca.2016.03.013

842   Schoenberg R., Zink S., Staubwasser M., von Blanckenburg F. (2008) The stable Cr isotope inventory
843   of solid Earth reservoirs determined by double spike MC-ICP-MS. *Chem. Geol.* **249**, 294–306.
844   https://doi.org/10.1016/j.chemgeo.2008.01.009

845   Shen J., Qin L., Fang Z., Zhang Y., Liu J., Liu W., Wang F., Xiao Y., Yu H., Wei S. (2018) High-
846   temperature inter-mineral Cr isotope fractionation: A comparison of ionic model predictions and
847   experimental investigations of mantle xenoliths from the North China Craton. *Earth Planet. Sci. Lett.*
848   **499**, 278–290. https://doi.org/10.1016/j.epsl.2018.07.041

849   Shen, J., Xia, J., Qin, L., Carlson, R. W., Huang, S., Helz, R. T., Mock, T. D. (2020) Stable chromium
850   isotope fractionation during magmatic differentiation: Insights from Hawaiian basalts and implications
851   for planetary redox conditions. *Geochim. Cosmochim. Acta.* **278**, 289-304.
852   https://doi.org/10.1016/j.gca.2019.10.003

853   Sossi P. A., Moynier F., van Zuilen K. (2018) Volatile loss following cooling and accretion of the
854   Moon revealed by chromium isotopes. *Proc. Natl. Acad. Sci.* U. S. A. **115**, 10920–10925.
855   https://doi.org/10.1073/pnas.1809060115

856   Sossi P. A., Klemme S., O'Neill H. S. C., Berndt J., Moynier F. (2019) Evaporation of moderately
857   volatile elements from silicate melts: experiments and theory. *Geochim. Cosmochim. Acta* **260**, 204–
858   231. https://doi.org/10.1016/j.gca.2019.06.021

859   Stormer, J. C., (1983) The effects of recalculation on estimates of temperature and oxygen fugacity
860   from analyses of multicomponent iron-titanium oxides. Am. Mineral. **68**, 586–594.

861 Suzuki A. M., Yasuda A., Ozawa K. (2008) Cr and Al diffusion in chromite spinel: Experimental
862 determination and its implication for diffusion creep. *Phys. Chem. Miner.* **35**, 433–445.
863 https://doi.org/10.1007/s00269-008-0238-2

864 Trinquier A., Birck J. L., Allègre C. J. (2008) High-precision analysis of chromium isotopes in
865 terrestrial and meteorite samples by thermal ionization mass spectrometry. *J. Anal. At. Spectrom.* **23**,
866 1565–1574. https://doi.org/10.1039/b809755k

867 Warren J. M. (2016) Global variations in abyssal peridotite compositions. *Lithos* **248**, 193–219.
868 https://doi.org/10.1016/j.lithos.2015.12.023

869 Williams H. M., McCammon C. A., Peslier A. H., Halliday A. N., Teutsch N., Levasseur S., Burg J.
870 P. (2004) Iron isotope fractionation and the oxygen fugacity of the mantle. *Science* **304**, 1656–1659.
871 https://doi.org/10.1126/science.1095679

872 Wood B. J., Virgo D. (1989) Upper mantle oxidation state: Ferric iron contents of Iherzolite spinels by
873 57Fe Mössbauer spectroscopy and resultant oxygen fugacities. *Geochim. Cosmochim. Acta* **53**, 1277–
874 1291. https://doi.org/10.1016/0016-7037(89)90062-8

875 Wood B. J., Bryndzia L. T., Johnson K.E. (1990) Mantle oxidation state and its relationship to tectonic
876 environment and fluid speciation. *Science*, **248**, 337–345.

877 Xia J., Qin L., Shen J., Carlson R. W., Ionov D. A., Mock T. D. (2017) Chromium isotope
878 heterogeneity in the mantle. *Earth Planet. Sci. Lett.* **464**, 103–115.
879 https://doi.org/10.1016/j.epsl.2017.01.045

880 Young E. D., Manning C. E., Schauble E. A., Shahar A., Macris C. A., Lazar C., Jordan M. (2015)
881 High-temperature equilibrium isotope fractionation of non-traditional stable isotopes: Experiments,
882 theory, and applications. *Chem. Geol.* **395**, 176–195. https://doi.org/10.1016/j.chemgeo.2014.12.013

883 Zhu J. M., Wu G., Wang X., Han G., Zhang L. (2018) An improved method of Cr purification for high
884 precision measurement of Cr isotopes by double spike MC-ICP-MS. *J. Anal. At. Spectrom.* **33**, 809–
885 821. https://doi.org/10.1039/c8ja00033f

886 Zhu, K., Sossi, P.A., Siebert, J., Moynier, F., Tracking the volatile and magmatic history of Vesta
887 from chromium stable isotope variations in eucrite and diogenite meteorites. *Geochim. Cosmochim.*
888 *Acta* 266, 2019, 598–610, https://doi.org/10.1016/j.gca.2019.07.043.

889

890

891

892

893

894

895

896

897

898

900
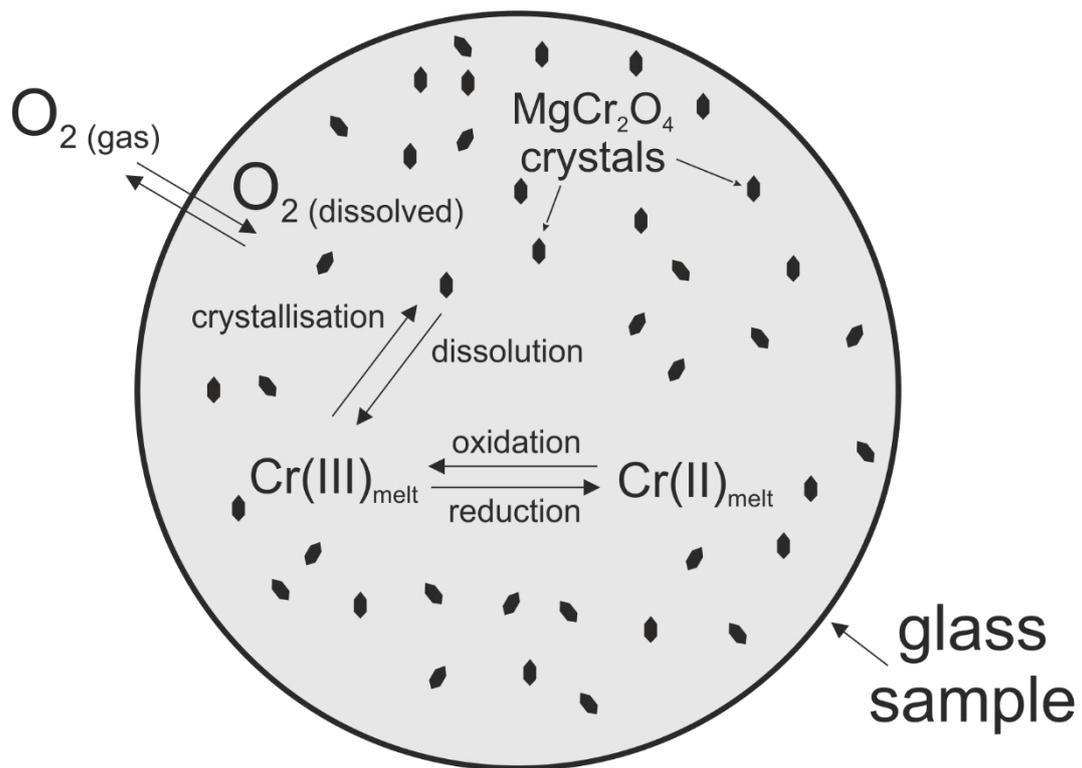
Figure 1: Schematic description of the reactions occurring during the experiments performed in this study. In the series A experiments, the magnesiochromite dissolve as Cr^{3+} in the silicate melts and depending on the redox conditions are reduced to Cr^{2+}. In the series B experiments, the magnesiochromite crystallised from the silicate melts. Figure modified from Khedim et al. (2008).
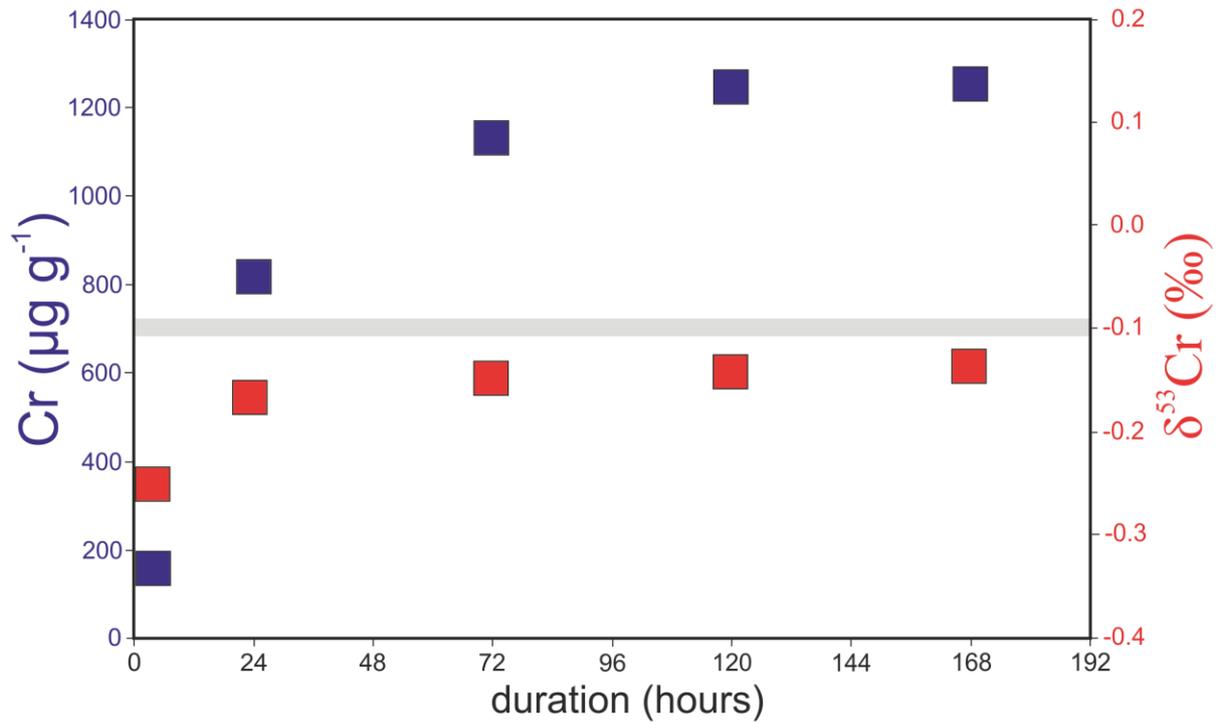
905

906 **Figure 2**: Chromium concentrations in the silicate melts versus time. The experiments shown in this

907 figure form part of the time series experiments (A3, A3a, A3b, A3c and A3d). The grey horizontal bar

908 is the Cr isotopic composition of the chromite at the start of the time series experiments. The blue and

909 red squares are the Cr concentration and Cr isotopic composition in the silicate melt of the time series

910 experiments, respectively.

911
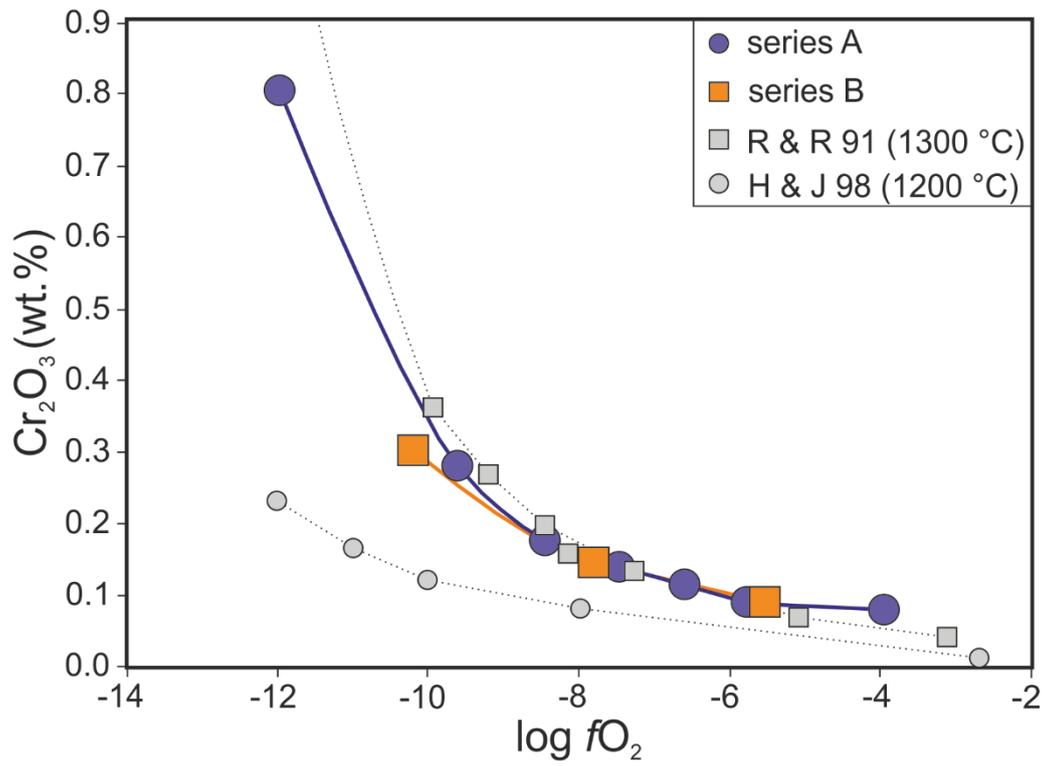
Figure 3: Cr chemical compositions in the silicate melts of series A and B experiments. The grey and

yellow data in (a) are from Roeder and Reynolds (1991) and Hanson and Jones (1998), respectively.
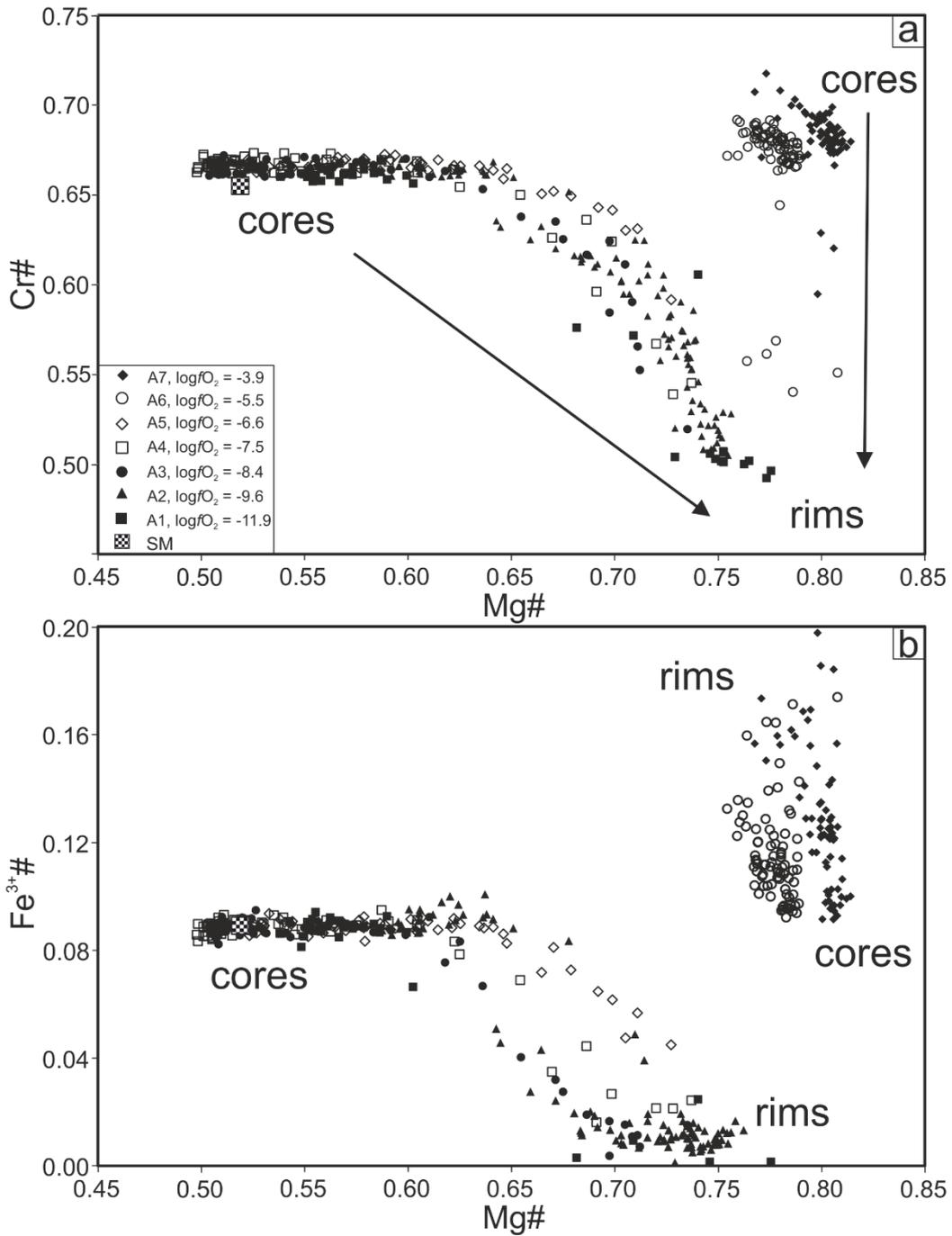
Figure 4: Cr# (a) and Fe^{3+}# (b) for the chromite in the series A experiments. The checkered square is the composition of the starting material (SM). Note that the most oxidised experiments produced rims substantially poorer in Cr and richer in Fe^{3+} than the cores.
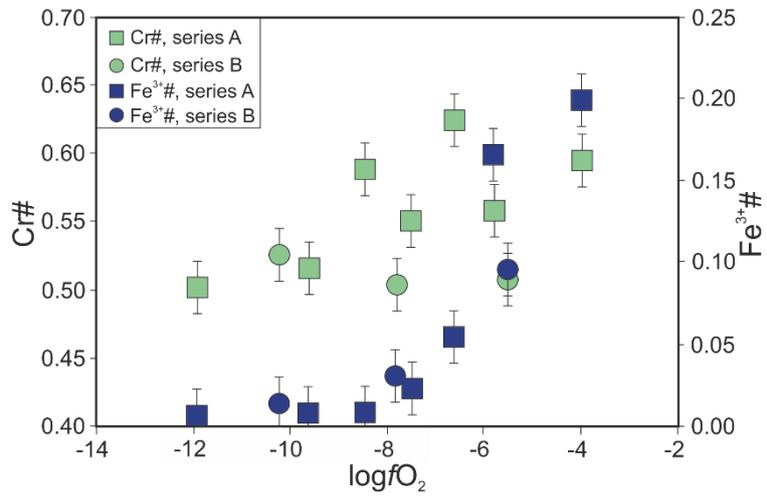
918

919 **Figure 5**: Cr number (green) and Fe^{3+}# (blue) in the rim (or small) chromite versus oxygen fugacity.

920
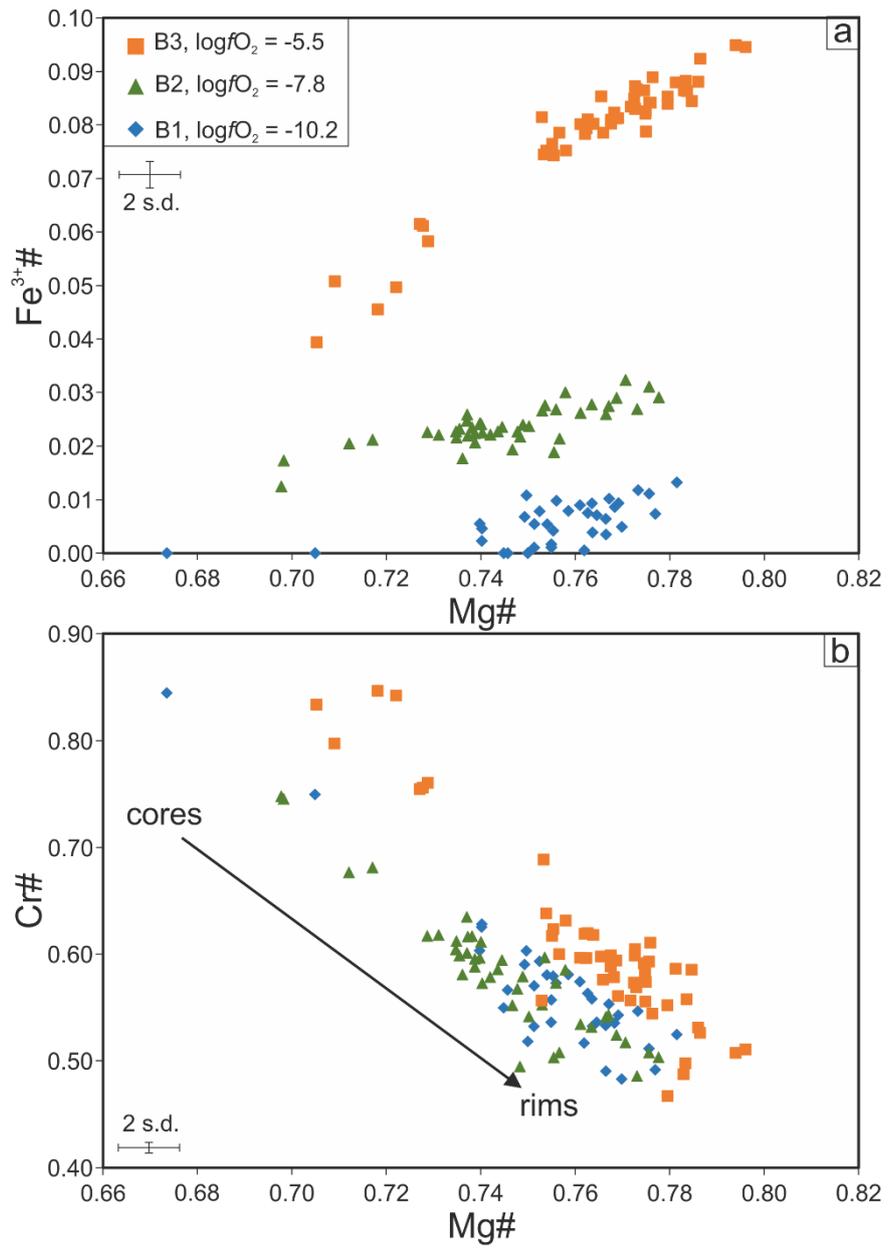
Figure 6: Fe^{3+}# (a) and Cr# (b) for the chromite in the series B experiments.

922
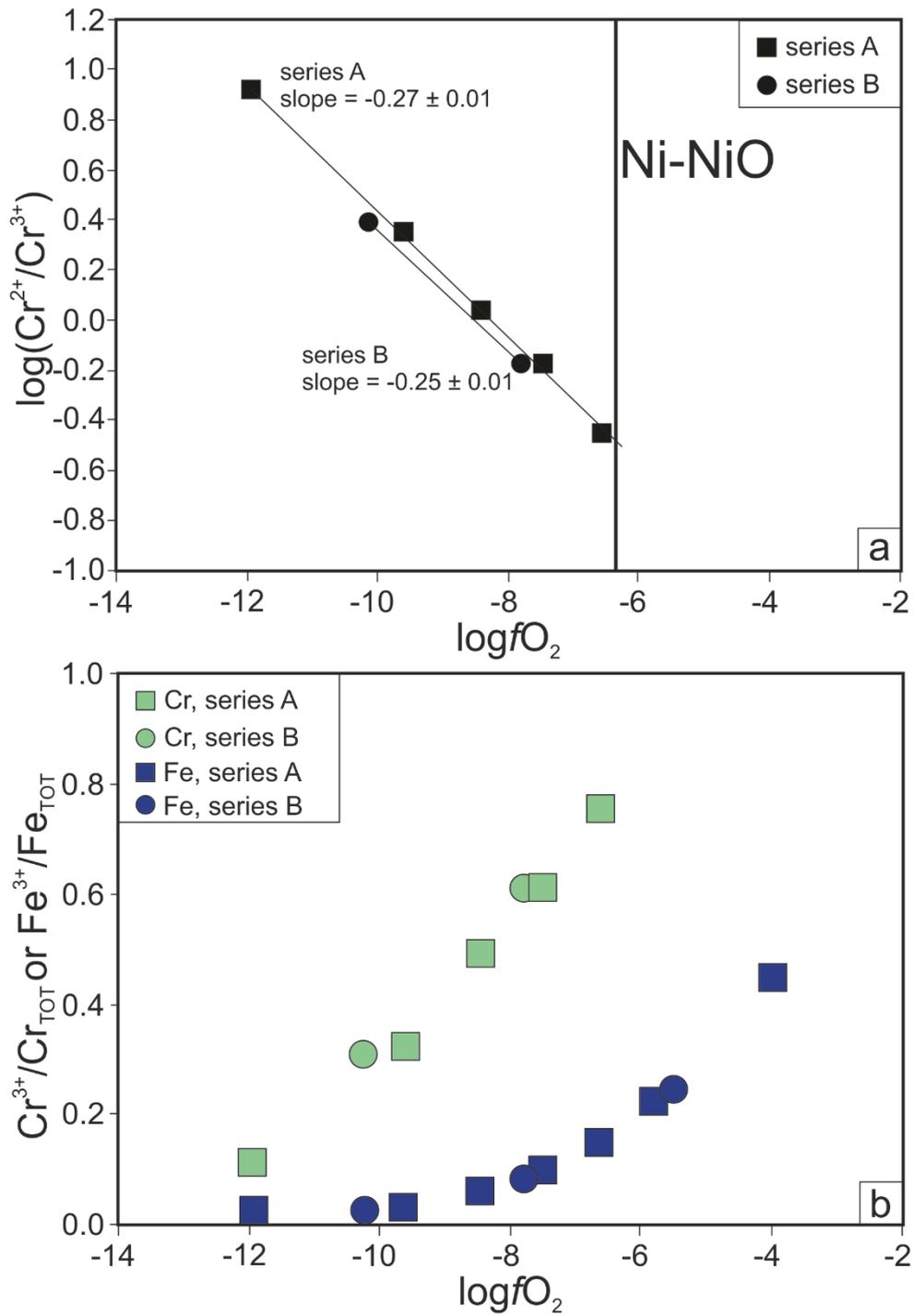
Figure 7: *Log*(Cr^{2+}/Cr^{3+}) (a) and Cr^{3+}/Cr_{TOT} (b) in the silicate melts versus *log* of oxygen fugacity. In

(b), in blue, Fe^{3+}/Fe_{TOT} in the silicate melts calculated with O'Neill (2018).

925
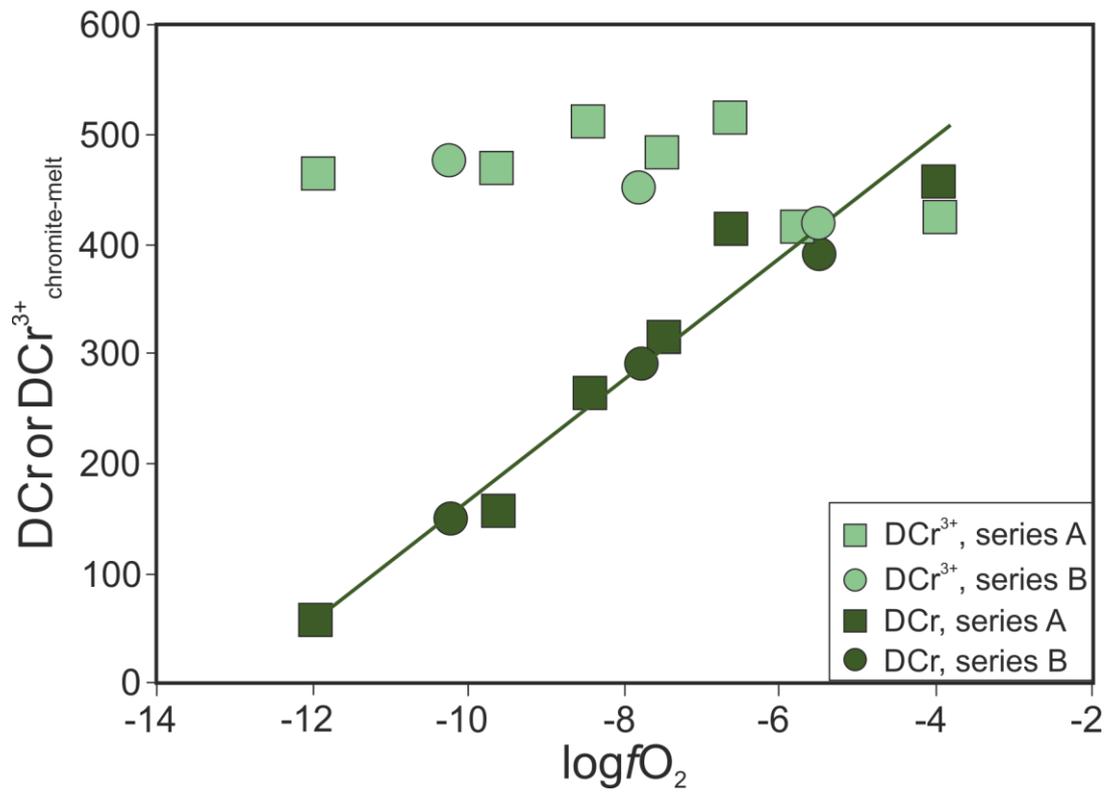
Figure 8: Partition coefficients $DCr_{chromite-melt}$ (dark green) and $DCr^{3+}_{chromite-melt}$ (light green) versus

oxygen fugacity. The square and round symbols are series A and B experiments, respectively.

928
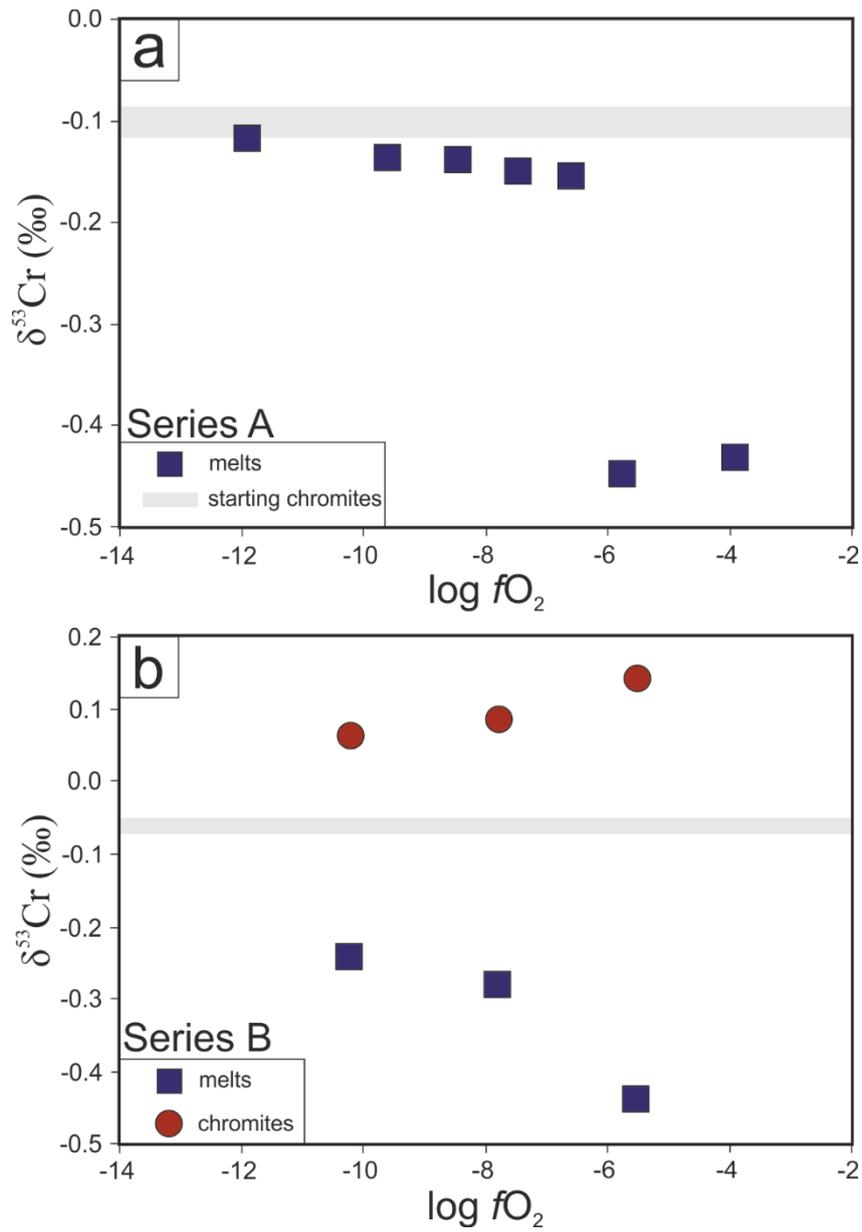
Figure 9: Cr isotopic compositions versus log*f*O₂ in series A (a) and series B (b) experiments. The red

circles are chromite and the blue squares are silicate melts. The grey bar in (a) is the Cr isotopic

composition of the chromite used as the starting material in the series A experiments.

932
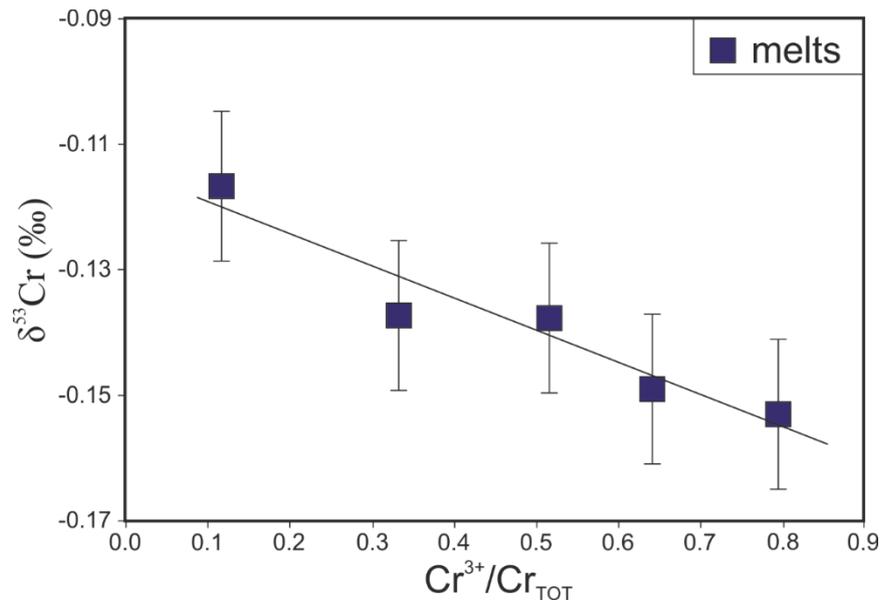
Figure 10: Chromium isotopic composition versus the Cr^{3+}/Cr_{TOT} ratio in the series A experiments

934   performed at $\log fO_2 < -6$.

935

936

937

938

939

940
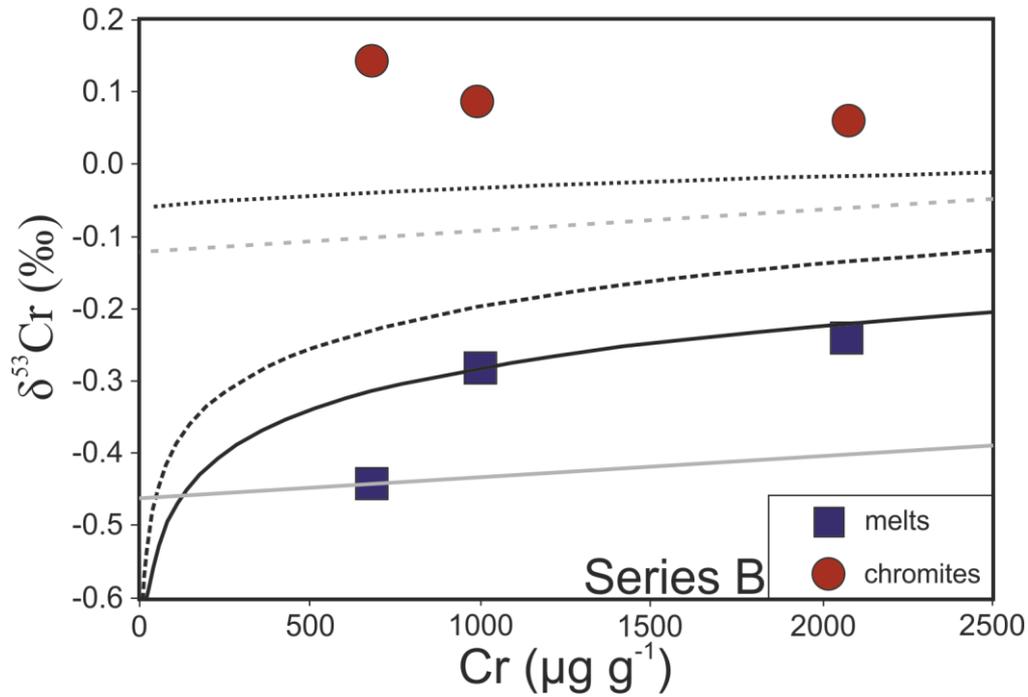
Figure 11: Chromium isotopic composition of melts and chromite versus Cr concentration for the

silicate melts of the series B experiments. The black lines correspond to a Rayleigh fractionation

model performed with a fractionation factor of 0.085. The solid black line is the silicate melt isotopic

composition. The dashed and dotted black lines are the instantaneous and cumulative chromite

isotopic composition, respectively. The grey lines are an equilibrium fractionation model. The solid

and dashed grey lines are the silicate melt and chromite isotopic compositions, respectively. For this

model, we used $\delta^{53}Cr_{chromite} - \delta^{53}Cr_{melt} = 0.4$ ‰. In both models, the starting Cr concentration is 13500

μg g^{-1}.The blue squares and red circles show the isotopic compositions of the coexisting silicate melts

and chromite, respectively.

958   Table 1: Average chemical composition of the starting silicate melts in series A and B experiments.

Wt. %	Series A	2 s.d.	Series B	2 s.d.
MgO	11.78	0.17	11.74	0.25
Al_2O_3	15.59	0.15	15.39	0.29
SiO_2	47.22	0.31	45.78	0.43
Cr_2O_3	n.d.	n.d.	1.97	0.04
FeO	7.36	0.11	7.41	0.21
CaO	17.58	0.16	17.43	0.45
Total	99.53	0.38	99.72	0.51

959

960

961

962

963

964

965

966

967

968

969

970

971

972

973

974

975

976

977

978

979

980

981

982

983   Table 2: Experimental settings for series A and B experiments.

series A	T (°C)	P (bar)	log$f$O$_2$	ΔQFM	Loop	time (hours)
A1	1300	1	-11.9	-4.57	Re	168
A2	1300	1	-9.6	-2.26	Re	168
A3	1300	1	-8.4	-1.09	Pt	168
A4	1300	1	-7.5	-0.13	Pt	168
A5	1300	1	-6.6	0.74	Pt	168
A6	1300	1	-5.8	1.58	Pt	168
A7	1300	1	-3.9	3.40	Pt	168
Time series						time (hours)
A3a	1300	1	-8.4	-1.09	Pt	2
A3b	1300	1	-8.4	-1.09	Pt	24
A3c	1300	1	-8.4	-1.09	Pt	72
A3d	1300	1	-8.4	-1.09	Pt	120
A3	1300	1	-8.4	-1.09	Pt	168
Series B						time (hours)
B1	1300	1	-10.2	-2.86	Pt	168
B2	1300	1	-7.8	-0.46	Pt	168
B3	1300	1	-5.5	1.84	Pt	168

984

985

986

987

988

989

990

991

992

993

994

995

996

997

998

999

1000

1001 Table 3: Major element concentration (wt. %) of the silicate melts in the series A and B experiments

Series A	MgO	2 s.d.	Al_2O_3	2 s.d.	SiO_2	2 s.d.	Cr_2O_3	2 s.d.	FeO	2 s.d.	CaO	2 s.d.	Total	2 s.d.	NBO/T	Fe^{3+}/Fe^{2+}	Fe^{3+}/Fe_{TOT}	Cr^{2+}/Cr^{3+}	Cr^{3+}/Cr_{TOT}
A1	11.89	0.15	15.50	0.22	47.30	0.24	0.81	0.04	6.77	0.16	17.52	0.16	99.79	0.41	0.53	0.01	0.01	7.64	0.12
A2	11.76	0.12	15.41	0.08	46.99	0.57	0.28	0.01	7.44	0.12	17.61	0.16	99.49	0.66	0.55	0.03	0.03	2.01	0.33
A3	11.75	0.14	15.50	0.21	47.32	0.22	0.18	0.01	7.34	0.15	17.57	0.13	99.66	0.52	0.54	0.06	0.06	0.95	0.51
A4	11.79	0.08	15.24	0.18	47.34	0.26	0.15	0.01	7.42	0.12	17.49	0.10	99.42	0.28	0.55	0.10	0.09	0.56	0.64
A5	11.61	0.09	15.48	0.11	47.30	0.35	0.12	0.01	7.43	0.09	17.48	0.15	99.41	0.50	0.54	0.17	0.15	0.26	0.79
A6	11.44	0.10	15.36	0.13	46.93	0.26	0.09	0.02	7.66	0.18	17.62	0.08	99.10	0.31	0.55	0.28	0.22	0.00	1.00
A7	11.56	0.07	15.35	0.13	47.20	0.21	0.09	0.02	7.63	0.12	17.54	0.18	99.38	0.18	0.55	0.80	0.44	-0.07	1.07
Time series																			
A3a	11.79	0.10	15.63	0.20	47.20	0.39	0.02	0.03	7.34	0.07	17.64	0.12	99.62	0.53	0.54	0.06	0.06	N/A	N/A
A3b	11.80	0.15	15.59	0.13	47.23	0.26	0.12	0.05	7.37	0.14	17.58	0.13	99.67	0.35	0.54	0.06	0.06	N/A	N/A
A3c	11.79	0.16	15.61	0.12	47.20	0.23	0.16	0.01	7.42	0.08	17.55	0.11	99.72	0.37	0.54	0.06	0.06	N/A	N/A
A3d	11.76	0.25	15.54	0.12	47.24	0.26	0.18	0.02	7.38	0.12	17.52	0.22	99.62	0.26	0.54	0.06	0.06	N/A	N/A
A3	11.75	0.14	15.50	0.21	47.32	0.22	0.18	0.01	7.34	0.15	17.57	0.13	99.66	0.52	0.54	0.06	0.06	1.10	0.48
series B																			
B1	11.62	0.21	15.26	0.17	47.43	0.36	0.30	0.06	6.82	0.18	18.05	0.33	99.57	0.64	0.55	0.02	0.02	2.25	0.31
B2	11.56	0.20	15.21	0.24	47.17	0.41	0.15	0.03	7.38	0.25	17.98	0.28	99.59	0.55	0.56	0.09	0.08	0.57	0.64
B3	11.36	0.34	15.12	0.46	46.84	0.52	0.10	0.03	7.35	0.21	17.83	0.75	99.43	1.67	0.58	0.32	0.24	0.07	0.93

1002 Fe^{3+}/Fe_{TOT} and Fe^{3+}/Fe^{2+} are calculated from O'Neill (2018), Cr^{3+}/Cr_{TOT} and Cr^{2+}/Cr^{3+} are calculated using Hanson and Jones (1998) method. See text for
1003 details.

1004

1005

1006

1007   Table 4: Chemical composition of selected chromite (wt. %) in the series A and B experiments. For each experiment, core and rim compositions are reported.

series A		MgO	Al$_2$O$_3$	TiO$_2$	Cr$_2$O$_3$	FeO	MnO	Total	Mg#	Cr#	Fe^{3+}#
A1	core	12.11	16.20	0.51	47.41	23.32	0.19	99.8	0.56	0.66	0.09
	rim	17.50	29.00	0.02	43.54	9.89	0.07	100.2	0.76	0.50	0.00
A2	core	13.02	16.10	0.51	47.98	22.04	0.14	99.9	0.60	0.67	0.09
	rim	17.08	27.75	0.01	43.97	10.96	0.04	100.2	0.75	0.52	0.01
A3	core	10.85	15.96	0.50	47.21	25.00	0.23	99.8	0.51	0.67	0.09
	rim	15.50	22.52	0.22	47.81	12.23	0.06	98.9	0.70	0.59	0.01
A4	core	10.82	15.82	0.50	47.59	24.97	0.23	100.0	0.51	0.67	0.09
	rim	16.48	24.87	0.16	45.40	12.72	0.06	100.1	0.73	0.55	0.02
A5	core	12.42	15.99	0.50	48.14	22.85	0.18	100.1	0.57	0.67	0.09
	rim	15.80	19.59	0.40	48.42	15.65	0.10	100.2	0.71	0.62	0.05
A6	core	17.54	16.05	0.50	49.20	16.20	0.08	99.6	0.78	0.67	0.10
	rim	17.95	20.79	0.05	38.98	21.77	0.04	99.8	0.78	0.56	0.17
A7	core	18.22	16.18	0.52	50.20	15.00	0.06	100.2	0.81	0.68	0.10
	rim	18.66	18.16	0.06	39.75	23.17	0.04	100.2	0.80	0.60	0.20
series B											
B1	core	13.85	8.02	0.03	64.91	11.95	0.00	98.7	0.67	0.84	0.00
	rim/small	17.86	27.01	0.00	44.48	9.97	0.06	100.0	0.78	0.53	0.01
B2	core	14.73	13.20	0.01	58.37	12.30	0.06	98.7	0.70	0.75	0.01
	rim/small	17.92	28.06	0.00	42.43	11.75	0.05	100.7	0.78	0.50	0.03
B3	core	14.67	8.36	0.00	62.37	13.80	0.06	99.3	0.71	0.83	0.04
	rim/small	18.20	25.46	0.00	39.12	15.87	0.05	99.2	0.80	0.51	0.10

1008

1009

1010

1011   Table 5: Cr isotopic composition for the silicate melts and the chromite for the series A and B
1012   experiments.

series A	$logfO_2$	$\delta^{53}Cr_{melt}$	2 s.e.	$\delta^{53}Cr_{chromite}$	2 s.e.
A1	-11.9	-0.117	0.006	-0.110	0.006
A2	-9.6	-0.137	0.005	n.d.	n.d.
A3	-8.4	-0.138	0.005	-0.115	0.004
A4	-7.5	-0.149	0.005	n.d.	n.d.
A5	-6.6	-0.153	0.004	n.d.	n.d.
A6	-5.8	-0.449	0.005	-0.102	0.009
A7	-3.9	-0.431	0.005	-0.108	0.009
Time series					
A3a	-8.4	-0.251	0.018	n.d.	n.d.
A3b	-8.4	-0.167	0.007	n.d.	n.d.
A3c	-8.4	-0.147	0.005	n.d.	n.d.
A3d	-8.4	-0.143	0.005	n.d.	n.d.
A3	-8.4	-0.138	0.005	-0.115	0.004
series B					
B1	-10.2	-0.240	0.006	0.063	0.010
B2	-7.8	-0.274	0.006	0.088	0.011
B3	-5.5	-0.437	0.008	0.150	0.008
starting material		-0.060	0.007		
JP-1	N/A	-0.108	0.014*		

1013   * 2 s.d. n=8

1014

1015

1016